Defense Nuclear Agency
Alexandria, VA 22310-3398

AD-A283 209

DNA-TR-93-147

Multi-Beam Laser Interferometer for Plasma Density Measurements in a Plasma Erosion Opening Switch (PEOS)

Stephen F. Fulghum
Science Research Laboratory, Inc.
15 Ward Street
Somerville, MA 02143

July 1994

Technical Report

CONTRACT No. DNA 001-92-C-0098

Destroy this report when it is no longer needed. Do not return to sender.

PLEASE NOTIFY THE DEFENSE NUCLEAR AGENCY, ATTN: CSTI, 6801 TELEGRAPH ROAD, ALEXANDRIA, VA 22310-3398, IF YOUR ADDRESS IS INCORRECT, IF YOU WISH IT DELETED FROM THE DISTRIBUTION LIST, OR IF THE ADDRESSEE IS NO LONGER EMPLOYED BY YOUR ORGANIZATION.

DISTRIBUTION LIST UPDATE

This mailer is provided to enable DNA to maintain current distribution lists for reports. (We would appreciate your providing the requested information.)

NOTE:
Please return the mailing label from the document so that any additions, changes, corrections or deletions can be made easily.

☐ Add the individual listed to your distribution list.

☐ Delete the cited organization/individual.

☐ Change of address.

NAME: _____

ORGANIZATION: _____

OLD ADDRESS	CURRENT ADDRESS
_____	_____
_____	_____
_____	_____

TELEPHONE NUMBER: ( ) _____

DNA PUBLICATION NUMBER/TITLE	CHANGES/DELETIONS/ADDITIONS, etc. *(Attach Sheet if more Space is Required)*
_____	_____
_____	_____
_____	_____

DNA OR OTHER GOVERNMENT CONTRACT NUMBER: _____

CERTIFICATION OF NEED-TO-KNOW BY GOVERNMENT SPONSOR (if other than DNA):

SPONSORING ORGANIZATION: _____

CONTRACTING OFFICER OR REPRESENTATIVE: _____

SIGNATURE: _____

CUT HERE AND RETURN

DEFENSE NUCLEAR AGENCY
ATTN: TITL
6801 TELEGRAPH ROAD
ALEXANDRIA, VA 22310-3398

DEFENSE NUCLEAR AGENCY
ATTN: TITL
6801 TELEGRAPH ROAD
ALEXANDRIA, VA 22310-3398

REPORT DOCUMENTATION PAGE

Form Approved OMB No. 0704-0188

1. AGENCY USE ONLY (Leave blank)	2. REPORT DATE	3. REPORT TYPE AND DATES COVERED
	940701	Technical 920825 – 931130

4. TITLE AND SUBTITLE

Multi-Beam Laser Interferometer for Plasma Density Measurements in a Plasma Erosion Opening Switch (PEOS)

5. FUNDING NUMBERS

C - DNA 001-92-C-0098
PE - 62715H
PR - AF
TA - DE
WU - DH326330

6. AUTHOR(S)

Stephen F. Fulghum

7. PERFORMING ORGANIZATION NAME(S) AND ADDRESS(ES)

Science Research Laboratory, Inc.
15 Ward Street
Somerville, MA 02143

8. PERFORMING ORGANIZATION REPORT NUMBER

SRL-11-F-1993

9. SPONSORING/MONITORING AGENCY NAME(S) AND ADDRESS(ES)

Defense Nuclear Agency
6801 Telegraph Road
Alexandria, VA 22310-3398
TDSP/Massman

10. SPONSORING/MONITORING AGENCY REPORT NUMBER

DNA-TR-93-147

11. SUPPLEMENTARY NOTES

This work was sponsored by the Defense Nuclear Agency under RDT&E RMC Code B4662D AF DE 00015 7010A AF 25904D.

12a. DISTRIBUTION/AVAILABILITY STATEMENT

Approved for public release; distribution is unlimited.

12b. DISTRIBUTION CODE

13. ABSTRACT *(Maximum 200 words)*

Science Research Laboratory has designed and fabricated a wide-bandwidth, highly sensitive, optical diagnostic for the simultaneous measurement of electron density and neutral gas density in plasma opening switches. The system uses two Mach-Zehnder interferometers, installed on a common support structure, to probe the refractive index of the plasma at 532 nm and 1064 nm along a common, 1-meter line-of-sight. Measurements at two wavelengths permit the effects of free electrons to be deconvolved from the effects of neutral gas species. The diagnostic is sensitive to fringe shifts of from 2×10^{-5} waves to 0.2 waves at bandwidths of up to 100 MHz. This allows the measurement of electron density path integrals from 5×10^{12} cm^{-2} to 5×10^{16} cm^{-2} with risetimes below 5 ns. The completed system was installed and tested on the HAWK facility at the Naval Research Laboratory in September 1993. Data is presented on the temporal history of the electron and neutral density path integrals in HAWK.

14. SUBJECT TERMS

Optical, Electron, Two-Color, Density, Measurement, Interferometer

15. NUMBER OF PAGES

94

16. PRICE CODE

17. SECURITY CLASSIFICATION OF REPORT	18. SECURITY CLASSIFICATION OF THIS PAGE	19. SECURITY CLASSIFICATION OF ABSTRACT	20. LIMITATION OF ABSTRACT
UNCLASSIFIED	UNCLASSIFIED	UNCLASSIFIED	SAR

CLASSIFIED BY:

N/A since Unclassified.

DECLASSIFY ON:
N/A since Unclassified.

CONVERSION TABLE

Conversion factors for U.S. customary to metric (SI) units of measurement

To Convert From	To	Multiply
angstrom	meters (m)	1.000 000 X E-10
atmosphere (normal)	kilo pascal (kPa)	1.013 25 X E+2
bar	kilo pascal (kPa)	1.000 000 X E+2
barn	meter^2 (m^2)	1.000 000 X E-28
British Thermal unit (thermochemical)	joule (J)	1.054 350 X E+3
calorie (thermochemical)	joule (J)	4.184 000
cal (thermochemical)/cm^2	mega joule/m^2(MJ/m^2)	4.184 000 X E-2
curie	giga becquerel (GBq)*	3.700 000 X E+1
degree (angle)	radian (rad)	1.745 329 X E-2
degree Fahrenheit	degree kelvin (K)	$t_K=(t^\circ f + 459.67)/1.8$
electron volt	joule (J)	1.602 19 X E-19
erg	joule (J)	1.000 000 X E-7
erg/second	watt (W)	1.000 000 X E-7
foot	meter (m)	3.048 000 X E-1
foot-pound-force	joule (J)	1.355 818
gallon (U.S. liquid)	meter^3 (m^3)	3.785 412 X E-3
inch	meter (m)	2.540 000 X E-2
jerk	joule (J)	1.000 000 X E+9
joule/kilogram (J/Kg) (radiation dose absorbed)	Gray (Gy)	1.000 000
kilotons	terajoules	4.183
kip (1000 lbf)	newton (N)	4.448 222 X E+3
kip/inch^2 (ksi)	kilo pascal (kPa)	6.894 757 X E+3
ktap	newton-second/m^2 (N-s/m^2)	1.000 000 X E+2
micron	meter (m)	1.000 000 X E-6
mil	meter (m)	2.540 000 X E-5
mile (international)	meter (m)	1.609 344 X E+3
ounce	kilogram (kg)	2.834 952 X E-2
pound-force (lbf avoirdupois)	newton (N)	4.448 222
pound-force inch	newton-meter (N·m)	1.129 848 X E-1
pound-force/inch	newton/meter (N/m)	1.751 268 X E+2
pound-force/foot^2	kilo pascal (kPa)	4.788 026 X E-2
pound-force/inch^2 (psi)	kilo pascal (kPa)	6.894 757
pound-mass (lbm avoirdupois)	kilogram (kg)	4.535 924 X E-1
pound-mass-foot^2 (moment of inertia)	kilogram-meter^2 (kg·m^2)	4.214 011 X E-2
pound-mass/foot^3	kilogram/meter^3 (kg/m^3)	1.601 846 X E+1
rad (radiation dose absorbed)	Gray (Gy)**	1.000 000 X E-2
roentgen	coulomb/kilogram (C/kg)	2.579 760 X E-4
shake	second (s)	1.000 000 X E-8
slug	kilogram (kg)	1.459 390 X E+1
torr (mm Hg, 0°C)	kilo pascal (kPa)	1.333 22 X E-1

*The becquerel (Bq) is the SI unit of radioactivity: Bp = 1 event/s.

**The Gray (Gy) is the SI unit of absorbed radiation.

TABLE OF CONTENTS

FIGURES

FIGURES (Continued)

SECTION 1

INTRODUCTION

1.1 OVERVIEW.

A major R&D effort is now underway to develop a new generation of above-ground, nuclear weapons effects simulators. Critical components in these simulators are the Plasma Erosion Opening Switch (PEOS) and numerous plasma sources required for their operation. An important parameter for the understanding of the operation of the PEOS is the density of the plasma (electrons and ions) within the switch. Experiments conducted in Phase I of this SBIR program at Science Research Laboratory (SRL) also indicated that neutral and excited species are present at critical times in the opening phase of these switches. The effects of these neutral states may be important to the understanding the physics of the opening phase. This Phase II SBIR was directed towards the development of a diagnostic to simultaneously measure the densities of electrons and neutral species. The resulting diagnostic is both more sensitive (resolves electron density path integrals below 10^{13} cm^{-2}) and faster (resolves density changes with risetimes of 3 nanoseconds) compared to previous diagnostic systems.

The design of the SRL plasma diagnostic is based on a Mach-Zehnder interferometer, set up to measure the change in the refractive index of the plasma at two separate wavelengths. Generally, the refractive index of the plasma is determined by both the density of free electrons and the density of neutral species. Free electrons result in a refractive index which is less than 1 (i.e. the phase velocity of the probe exceeds the speed of light) and an interferometric fringe shift which is proportional to the wavelength of the probe beam used. Neutral (and excited state) gas densities result in a refractive index which is greater than 1 and a fringe shift which is inversely proportional to the wavelength of the probe. By measuring the fringe shifts on probe beams at

two different wavelengths the contribution to the fringe shift from electrons can be separated from the contribution due to neutral species. The density of the electrons is definitely determined since the refractivity of free electrons is known. The density of the neutrals (there may be more than one species) is generally indicated since the refractivity of most neutral species is about the same.

Interferometric probes have long been used in various forms as plasma diagnostics. A higher bandwidth (but less sensitive) electron density diagnostic utilizing a single-color, Mach-Zehnder interferometer is described by Reilly[1]. More recent single-color diagnostics have generally used heterodyne detection, such as the HeNe laser system described by Weber[2], used on the HAWK PEOS at the Naval Research Laboratory (NRL). Heterodyne systems are generally easier to implement and have significant advantages where fringe shifts exceed 1 wave (path integrals of 10^{17} cm^{-2} and up) and where it is difficult to obtain a line-of-sight through the plasma. Implementations of heterodyne diagnostics to date, however, have been less sensitive than the SRL diagnostic system. Two-color laser interferometry has also been demonstrated previously by measuring the deflection of helium-neon and carbon-dioxide laser beams due to gradients in plasmas.[3] This deflection system, however, is much less sensitive that either the heterodyne or the direct phase shift measurement techniques. To our knowledge, the plasma diagnostic to be described is the first implementation of a two-color interferometer capable of measuring electron density path integrals below 10^{13} cm^{-2} at bandwidths of 100 MHz while providing simultaneous measurements of the neutral density along the same path.

This Final Report describes the two-color, interferometric plasma diagnostic developed and tested under this Phase II SBIR program and the results of its initial tests on the HAWK PEOS at the Naval Research Laboratory. More detail as to the basic theory of operation of this device as a diagnostic for electrons and gases can be found in the Phase I SBIR Final Report[4] and the Phase II Proposal[5] (with sections marked proprietary removed for distribution). A detailed description of the general design of the interferometer optics and detection system has been published.[6]

This Final Report provides an overview of the optical and mechanical design of the final system, concentrating on the differences between the system originally proposed and the system actually delivered. A paper describing the opto-mechanical design of the interferometer in detail will be published in the Review of Scientific Instruments at a later date. The results of the measurement performed on the HAWK PEOS at NRL are included, concentrating on what they indicate in terms of the system performance. Finally, this report indicates what changes should be implemented in the delivered design, based on the experience of the initial tests.

The Operations Manual for the instrument is included with this Final Report to avoid unnecessary duplication of text and figures. The Operations Manual focuses on the mechanical setup of the system, its optical alignment and the use of the detection electronics. The characteristics of the optical components and the detailed design of the electronics components are also described in case repairs or modifications must be made.

1.2 ADHERENCE TO STATEMENT OF WORK.

The specific tasks in the contract SOW are as follows:

Task 1: Design and Construction.

> The contractor shall design and construct a multi-beam laser interferometer system capable of measuring electron and neutral particle densities in plasmas. The interferometer system shall be capable of being adapted to the POS within the Naval Research Laboratory (NRL) HAWK facility in each of three configurations: (1) single-wavelength and single-beam for measurement of electron density, (2) single-wavelength and multiple-beam for measurement of spatial variation of electron densities, and (3) two-beam for simultaneous measurement of electron density and neutral particle density.

This task was completed in its entirety. The final system, as installed on HAWK, combines all three mode of operation into the same optical setup. The adjustment of two sets of mirrors

determines whether the two interferometer probe beams are on the same axis (configuration 3) or on separate axes (configuration 2). Configuration 1 is thus just configuration 2 or 3 with one of the lasers turned off.

Task 2: Testing and Plasma Source Characterization.

> The contractor shall adapt the interferometer system to a flashboard test stand, test all aspects of interferometer operation, and characterize and analyze the performance of the NRL and Maxwell Laboratories Incorporated (MLI) designed plasma flashboards. Flashboard analysis shall be oriented toward identifying design measures to improve flashboard performance. Analysis of NRL flashboard performance shall include comparison with results of similar studies performed by NRL on the same design flashboards.

The flashboard test stand, with an NRL flashboard, was completed and installed on the plasma diagnostic at SRL for tests. The operational failure of a probe laser, however, prevented these experiments from being carried out. This SBIR contained the time constraint that all tests on the HAWK PEOS at NRL had to be carried out during FY93. The plasma diagnostic had to be disassembled and shipped to NRL before the probe laser could be repaired. The equivalent flashboard tests on the NRL flashboards were successfully completed on the HAWK facility as discussed below.

Task 3: Install and Test on HAWK.

> The contractor shall install and test the interferometer systems, in all three operating configurations noted in Task 1, on the POS of the HAWK simulator at NRL. Analysis of performance data shall include comparison with NRL plasma measurements within the HAWK POS using the NRL-designed He-Ne laser interferometer system under similar operating conditions.

The SRL diagnostic system (embodying all three operating configurations as described above) was successfully installed and tested on the HAWK PEOS. These tests concentrated on the two-color, overlapped path mode of operation (configuration 3) which could measure both electron and neutral species simultaneously. For comparison, the tests were conducted in a region of the HAWK PEOS where the electron density had been measured by Weber, et.al. using a HeNe heterodyne interferometer. The results of these tests are described below. NRL later tested the SRL diagnostic system (on their own) in a region where the heterodyne interferometer had not been sufficiently sensitive to determine the electron density. The electron densities measured in these tests have been provided to us by NRL for this report since they indicate the minimum detectable electron density that the SRL diagnostic can currently resolve. Tests with parallel beams along multiple chords (configuration 2) have not yet been made.

Task 4: Analysis and Report Preparation.

> The contractor shall analyze all aspects of interferometer performance for each mode of operation as performed during Tasks 2 and 3. The final technical report shall include, as a minimum, the results of this analysis with supporting test data, the analysis described in Tasks 2 and 3 with supporting test data, the designs and specifications for the interferometer system, and instructions for operation and maintenance of the interferometer.

This Final Report and Operations Manual generally fulfills the requirements of this final task.

1.3 MODIFICATIONS TO THE PROPOSED SYSTEM DESIGN.

The design of the SRL Plasma Diagnostic as delivered is very close to that proposed with two exceptions: (1) the wavelengths chosen for the probe lasers and (2) the way in which the two beams are combined onto a common axis.

The original design called for a krypton-ion laser to provide 300 mW at 647 nm for single color operation. Two-color operation was to use the krypton-ion laser on its 476.2 nm line combined with a small, 1 mW HeNe laser at 633 nm. Two krypton-ion lasers operating on different lines would have been optimal, but at 35K$ for each laser the cost was prohibitive.

After the Phase I experimental results were considered it became obvious that the two-color mode of operation, which would allow both electrons and neutrals to be measured, was critical to the success of the final diagnostic system. Also, while the Phase II proposal was being considered, diode-pumped Nd-YAG lasers appeared on the market at very competitive prices. The optimal choice for the probe lasers shifted to a 100 MW, diode-pumped, Nd-YAG laser at the fundamental 1064 nm wavelength and a 50 mW, diode-pumped, Nd-YAG laser at the doubled 532 nm wavelength. These diode-pumped lasers are far more compact, easier to operate, easier to maintain and less expensive than the krypton-ion laser in the original design. The two wavelengths are also exact multiples of each other which may prove essential in later applications (to be discussed). On the other hand, the krypton-ion laser was to have provided at least 300 mW of power at 647 nm. The added power would have allowed lower electron densities to be measured in the single-color mode of operation. In general, the switch to the diode-pumped lasers has turned out to be well advised.

The switch to a visible laser and a near-infrared laser for the two probes also required a modification of the original (Proprietary) design for the optics to combine the two probe beams onto a single axis. A simpler beam combining design, based on dichroic mirrors which pass the infrared beam and reflect the visible beam, also provides for more flexibility in the placement of the two probe beams. The SOW called for a diagnostic which could be operated in a mode with two, spatially separated probe beams as well as the mode in which two probes (of different colors) are placed onto the same axis. The use of the dichroic mirror beam combiners provides for both modes in the same optical configuration, depending on how the mirrors are aligned.

1.4 SUMMARY OF THE TEST RESULTS.

The SRL plasma diagnostic system operates as expected, resolving electron density path integrals below 10^{13} cm^{-2}. Electron density fall times of 15 ns (not instrument limited) were measured during the opening phase of the HAWK PEOS. Electron densities were measured in regions of the HAWK PEOS which were too low to be measured with the previous heterodyne diagnostic. Neutral densities are readily apparent in all of the HAWK test shots, including those in which only the flashboards were fired, those in which current was conducted through the plasma (normal operation) and those in which only the Marx banks were fired without firing the flashboards.

The electron densities measured for the NRL flashboards were very similar to the densities measured for the Maxwell flashboards in terms of both magnitude and temporal profile. The electron densities measured during the opening phase of the PEOS were very similar to those measured previously with the heterodyne diagnostic. The neutral densities were, of course, measured for the first time. The neutral densities in the opening switch tests rise rapidly as the switch opens to densities an order of magnitude greater than the electron density. These effects were masked in the single-color diagnostics by the much greater effect of the electrons on the plasma refractive index.

An "anomalous" refractive index shift, not entirely unexpected, complicates the analysis of this data in terms of only electrons and neutral gases. In most of the test shots there are brief periods during which neutral excited states, probably of carbon or hydrogen, are apparently formed. The effect of these states on the refractive index of the plasma causes the analysis program to indicate neutral densities which are negative (obviously unphysical). These periods occur relatively early as the plasma from the flashboards begins to ramp up. Since the exact

species and their concentrations are not known, their effects (which would otherwise be predictable) cannot be included in the model. These effects only occur when there are characteristic absorption lines, such as the H_α line at 656 nm, between the 532 nm probe wavelength and the 1064 nm probe wavelength. These effects could be minimized (or even exploited for additional information) by using a different wavelength for one or the other probe.

SECTION 2

INTERFEROMETER DESIGN OVERVIEW

2.1 EFFECT OF ELECTRONS AND NEUTRALS ON THE REFRACTIVE INDEX.

The SRL plasma diagnostic directly measures the phase difference, ϕ, between the reference beam and the scene beam at the exit of the interferometer. The reference beam is the beam passed around the plasma. The scene beam is the beam which has passed through the plasma. The output voltage signal from the diagnostic is directly proportional to $cos(\phi)$. Typically, the initial phase difference, ϕ_0, is set to $\pi/2$ (1/4 wave of relative path difference) before any data is taken. This is accomplished in the SRL system with a piezoelectric translator on one of the mirrors. This means that the initial voltage signal is zero and any subsequent change in the relative phase, $\delta\phi$, is proportional to $sin(\delta\phi)$. For small changes in the relative phase the signal voltage is then simply proportional to $\delta\phi$.

The phase change on a probe laser due to free electrons, $\delta\phi_e$, in a plasma is proportional both to the path integral of the electron density, n_e, and to the wavelength of the probe, λ.

$$\delta\phi_e = -r_e \lambda \int_0^L n_e \, dl$$

The phase change is negative since the phase velocity of the probe beam in a "gas" of free electrons is actually faster than the speed of light (no threat to causality- see your textbook). The proportionality constant, r_e (the classical radius of an electron), is equal to 2.82×10^{-13} cm. For the 1064 nm laser wavelength the conversion factor is 3×10^{-17} cm^2. A 10^{16} cm^{-3} electron density over a 10 cm path thus accounts for a phase change of 3 radians or about half a wave. This is about the electron density in HAWK at the time of opening.

The phase change on the probe laser due to neutral species, $\delta\phi_n$, is also proportional to the path integral of the neutral density, ρ, but inversely proportional to the probe wavelength

$$\delta\phi_n = 2\pi \frac{\beta}{\rho_0} \frac{1}{\lambda} \int_0^L \rho \, dl$$

Here the phase change is positive since the phase velocity of the probe beam in a "neutral" gas is less than the speed of light. The proportionality constants are β, the Gladstone-Dale constant for the gas and ρ_0, the gas density at which β is specified. Air, for example, has a refractive index, n, of about 1.0003 at a pressure of 1 atmosphere at room temperature. The value of β for air is thus about 3×10^{-4} with ρ_0 equal to about 2.5×10^{19} cm^{-3}. The total proportionality constant for air at a wavelength of 1.064 μm is thus 7×10^{-19} cm^3 compared to 3×10^{-17} for electrons. The effect of a single electron on a 1μm probe is thus about 40 times the effect of a single "air" molecule.

This is a good point at which to explicitly state a central assumption in the analysis of the "neutral" density as determined by this instrument. All species which can absorb light, including ions (with at least one electron), ground-state neutrals and excited-state neutrals will contribute to a positive refractive index. Note that hydrogen ions (protons), which are a likely constituent in these plasmas, do not absorb light and thus will not be detected as neutrals. When the hydrogen ions and electrons recombine the hydrogen atom will be detected. The refractive index of a given species is determined by the sum of all of its absorptions at all wavelengths and will vary with wavelength. If there are no strong absorption lines between or near the two probe wavelengths, then the refractive index at the two wavelengths will be about the same. The analysis presented in this Final Report assumes that the refractive index is the same at both wavelengths. Specifically, the value for β/ρ_0 is assumed to be 1×10^{-23}, or about the refractivity of air. If more information is obtained as to the identity of the absorbing species in the plasma then the analysis can be refined.

By measuring the phase shifts at two wavelengths, $\phi_I - \phi_{I0}$ and $\phi_G - \phi_{G0}$ (I for infrared and G for green), and by making the assumption described above, the path integral of the density of electrons, $n_e L$, and the path integral of the density of neutrals, ρL, can be determined as follows.

$$n_e L = \frac{1}{r_e} \frac{(\phi_I - phi_{I0})\lambda_I - (\phi_G - \phi_{G0})\lambda_G}{(\lambda_G^2 - \lambda_I^2)}$$

$$\rho L = \frac{\rho_0}{2\pi\beta} \frac{(\phi_I - phi_{I0})\lambda_G - (\phi_G - \phi_{G0})\lambda_I}{(\lambda_G/\lambda_I - \lambda_I/\lambda_G)}$$

There are many places in the optical train, detectors and electronics where the sign of the output signal is inverted. The solution above assumes that the signals at the digitizer, due to electrons, for BOTH the infrared and green probes, are negative relative to the baseline.

2.2 EFFECT OF DISPERSION ON THE ANALYSIS.

The analysis above assumes that the refractive index of the "neutral" species is the same at all wavelengths. This assumption is appropriate if the identity of the neutral species is not known. All species, however, exhibit dispersion which is the variation of refractive index with wavelength.

The classic model of dispersion found in most textbooks assumes that the electrons in a substance are bound to a nucleus as damped, simple harmonic oscillators.[7,8] The resulting complex refractive index, $\mathcal{N}$, for a light wave of frequency, ω, propagating through these bound electrons at a density N where a fractional population, f_j (the oscillator strength), has a characteristic oscillation frequency, ω_j, is given by

$$\mathcal{N}^2 = 1 + N\,(4\pi r_e c^2) \sum_j \left(\frac{f_j}{\omega_j^2 - \omega^2 - i\gamma_j\omega} \right).$$

The complex part of the refractive index simply means that the bound electron gas will absorb at the resonance frequencies or "lines" with a linewidth which depends on the damping constant, γ. Figure 2-1 shows schematically how the real part of the refractive index (which the interferometer will detect as a phase shift) varies for a substance with absorption bands in the UV, visible and infrared regions of the spectrum.[7]

At very short wavelengths (high frequencies) the bound electrons cannot respond to the rapidly varying electric field and have little effect on the propagation of the wave. The refractive index in this case is close to 1. The electrons can respond to low frequencies (long wavelengths) and slow the propagating wave (the refractive index is greater than 1). The refractive index drops to a more negative minimum approaching the absorption line center from the short wavelength side. The index then rises sharply to a more positive peak moving through the absorption line center towards longer wavelengths. The index drops back from its more positive peak but retains a net positive offset moving further to the red. The positive refractive index of materials transparent in the visible wavelength region can be considered as the sum of all of the positive offsets from absorptions in the ultraviolet. Generally these substances have refractive indices which slowly decrease with longer wavelengths since there are additional absorption bands in the infrared. This is considered to be "normal" dispersion. The rise in the refractive index when approaching an absorption line from the blue side is thus considered "anomalous" dispersion.

Generally, the absorption linewidths are narrow at the plasma densities of interest so it will be unlikely that a particular probe beam is very close to an absorption line. In this case the $\gamma_j\omega$ term is small compared to the $\omega_j^2 - \omega^2$ term and the refractive index can be approximated by

$$n^2 = 1 + N\,(4\pi r_e c^2)\,\sum_j \left(\frac{f_j}{\omega_j^2 - \omega^2}\right).$$

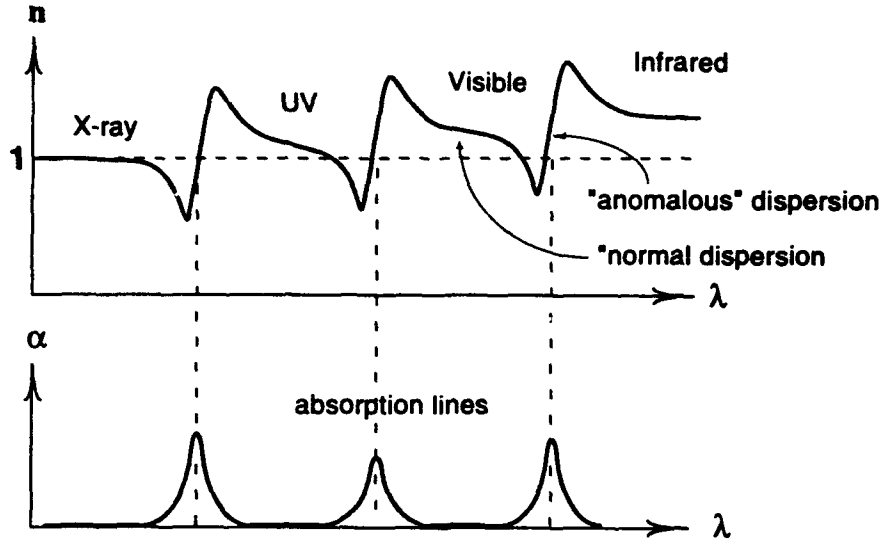

Figure 2-1: Index of refraction as a function of wavelength for a substance with absorption bands.[7]

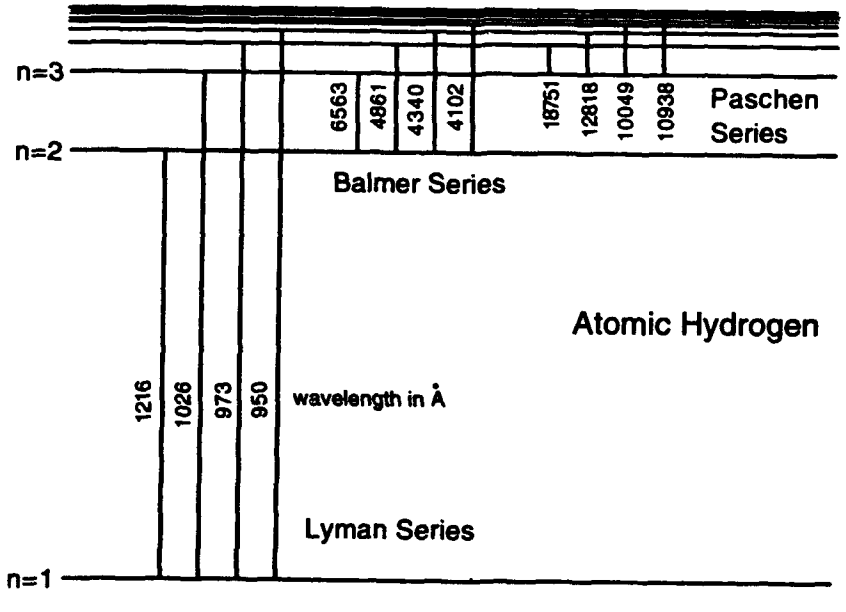

Figure 2-2: Absorption bands of excited atomic hydrogen.

2.3 EFFECT OF THE TRANSIENT SPECIES ON THE ANALYSIS.

It has been suggested that the plasma species from the HAWK flashboards are probably atomic hydrogen and carbon. The experimental results from HAWK presented below also indicate that the quantum states of these neutral species (and perhaps their actual identity and relative concentrations as well) change during opening switch runs. The absorption lines characteristic of a species change when its quantum state changes as shown in Fig. 2-2. Changing the characteristic absorption lines will, in general, change the refractive index of the plasma. If, for instance, some fraction of a gas of neutral hydrogen atoms are excited from their n=1 ground states to their n=2 excited states then its characteristic absorption lines change from the Lyman series in the ultraviolet to the Balmer series in the visible. Changing the state to n=3 changes the absorption lines to the Paschen series in the infrared. The changes in the refractive index would persist until the hydrogen drops back to its ground state with the emission of ultraviolet photons in the Lyman series.

Figure 2-3 shows the refractive index per atom for the three lowest energy states of hydrogen. These calculations[9] are based on the hydrogen spectral wavelengths and oscillator strengths given in Table 5.07.B.1 of Ref. 10.

Consider the effect of the 656.3 nm, H_α absorption line from the n=2 to n=3 state of atomic hydrogen. This absorption line lies midway between the 532 nm and 1064 nm probe wavelengths of our instrument. When a fraction of neutral ground state atomic hydrogen is excited to the n=2 state the net change in the refractive index at 1064 nm is positive and the net change at 532 nm is negative. Even a few percent conversion would be significant since the refractivity at either of these wavelengths is about 20 times greater than the refractivity of the ground state. A single wavelength experiment at 1064 nm would indicate a decrease in the electron density. A single wavelength probe at 532 nm would indicate an increase in the electron density. Note that a single wavelength probe at the 633 nm wavelength of a HeNe laser would

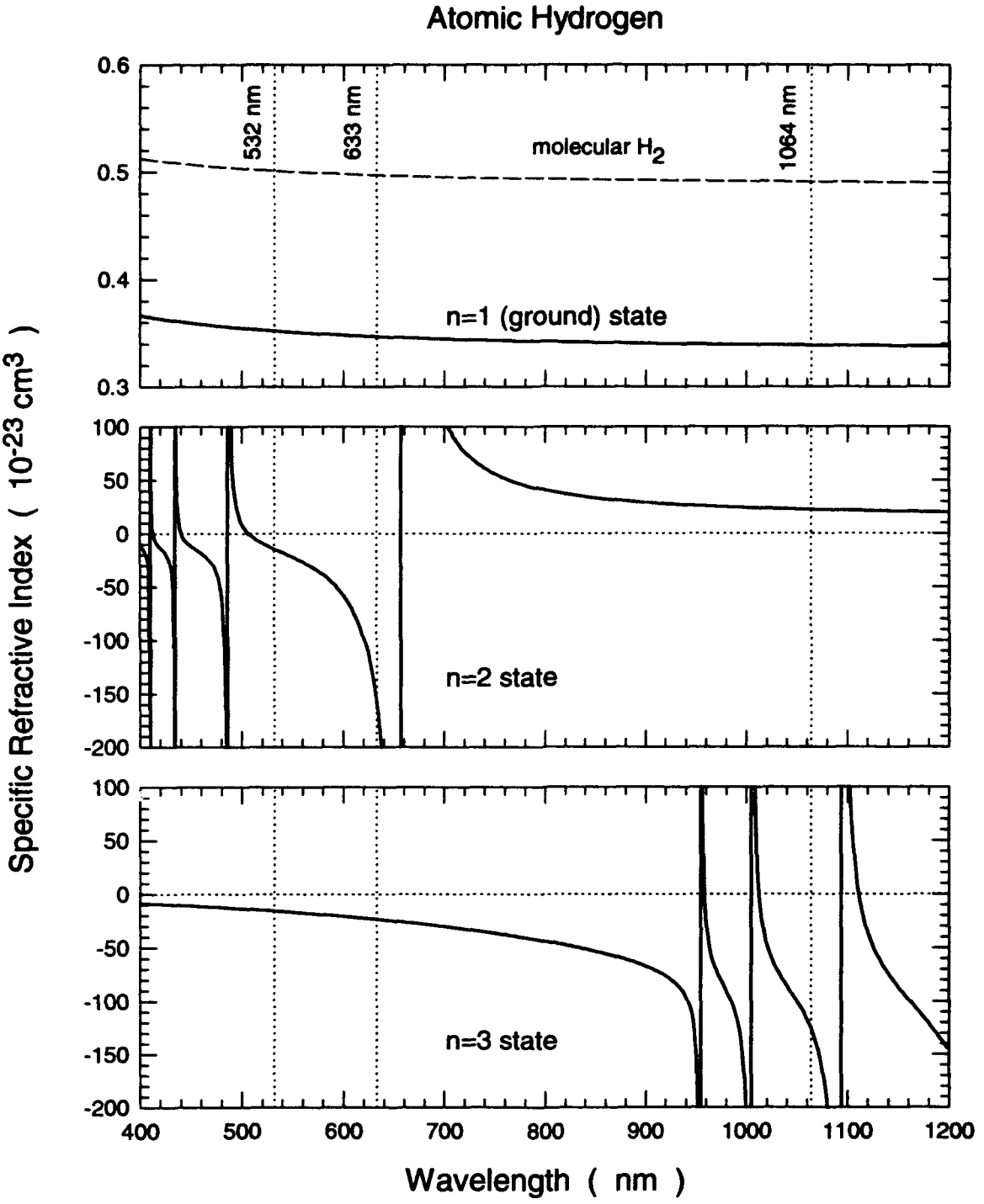

Figure 2-3: Dispersion of ground state and excited state atomic hydrogen.

indicate a large increase in the electron density since this wavelength is to the blue and relatively close to the H_α line.

If n=2 hydrogen is present, then analyzing data from both the 532 nm and 1064 nm probes simultaneously as described above will indicate an unphysical negative neutral density. This behavior in the data has been observed at times in the actual experiments to be described below. Whether this behavior is the result of excited hydrogen, excited carbon or other transient species is not known. A tunable probe laser would be able to distinguish these individual species by performing measurements below, at and above their resonance frequencies.

Note that ionized hydrogen atoms (protons) do not significantly affect the refractivity of the plasma because protons do not absorb light. The recombination of atomic hydrogen into molecular hydrogen also has relatively little effect on the refractive index because the refractivity of H_2 is about twice that of H.

2.4 INTERFEROMETER STABILITY REQUIREMENTS.

The design goal for the SRL interferometer was to detect a fringe shift of 10^{-5} waves in the visible, corresponding to a electron density path integral of about 4×10^{12} cm^{-2}. This fringe shift, if due to mirror vibration, would be equivalent to a mirror motion of less than 1/10 of an atomic diameter. Fortunately, the fringe shifts due to electrons in many plasmas of interest occur on much shorter time scales than the periods of vibrational modes in the interferometer structure. The structure must be sufficiently stable, however, to hold the relative path difference between the two arms of the interferometer close to the 1/4 wave condition for linear output signals. A tolerance of $\pm1/20$ wave is adequate. For small interferometers this is not difficult. The interferometer for the current application, however, is fairly large since it needs to reach around the four-foot diameter of the HAWK opening switch.

SRL has achieved the required stability in its interferometer by mounting the optical components on a frame composed of very stiff space trusses of stainless steel tubing as shown in

Fig. 2-4. A spring suspension, shown in Fig. 2-5, isolates the interferometer from vibrations in the external support structure and a vacuum chamber surrounding the interferometer isolates it from acoustic disturbances and thermal changes in the environment. Figure 2-6 shows a view inside the vacuum chamber down the horizontal path that the reference beams take through the horizontal space truss.

The interferometer structure has its own internal vibrational modes which are excited by residual vibrations coupled through the spring suspension system. Various forms of mass dampers are attached to the frame to convert the power in these vibrational modes to heat. Figure 2-7 shows a drawing of the final design of the SRL interferometer, suspended inside of its vacuum housing.

The vacuum chamber itself is also isolated from mechanical noise in the laboratory by a commercial vibration isolation system. This minimizes the motion of the support points for the spring suspension system which are, of course, attached to the vacuum chamber. In the NRL installation, this table is attached to the HAWK switch structure as shown in Fig. 2-8.

In the NRL tests this interferometer demonstrated a long term drift rate of about 0.001 waves per second. This means that the 1/4 wave condition for a linear output signal could be held within acceptable tolerances for about 1 minute without readjusting the piezoelectric translator. A feedback loop was built to lock the system at the 1/4 wave condition but was not required for the NRL tests.

Figure 2-9 shows the RMS amplitude of low frequency system noise after the linear drift cited above has been subtracted from the total. The peak vibrational amplitude of about 1 nm (0.001 waves at the 1064 nm probe wavelength) occurs at the suspension spring frequency of 1 Hz. No significant additional noise is evident at the primary internal modes of the structure which were measured with a laser vibrometer to be 8 Hz (torsional mode) and 20 Hz (bending mode). The noise at 1 kHz is due to cooling fan noise on the probe lasers. Above 1 kHz the dominant noise is due to shot noise and thermal noise in the fringe shift detection electronics.

Figure 2-4: Photograph of a space truss in the interferometer frame.

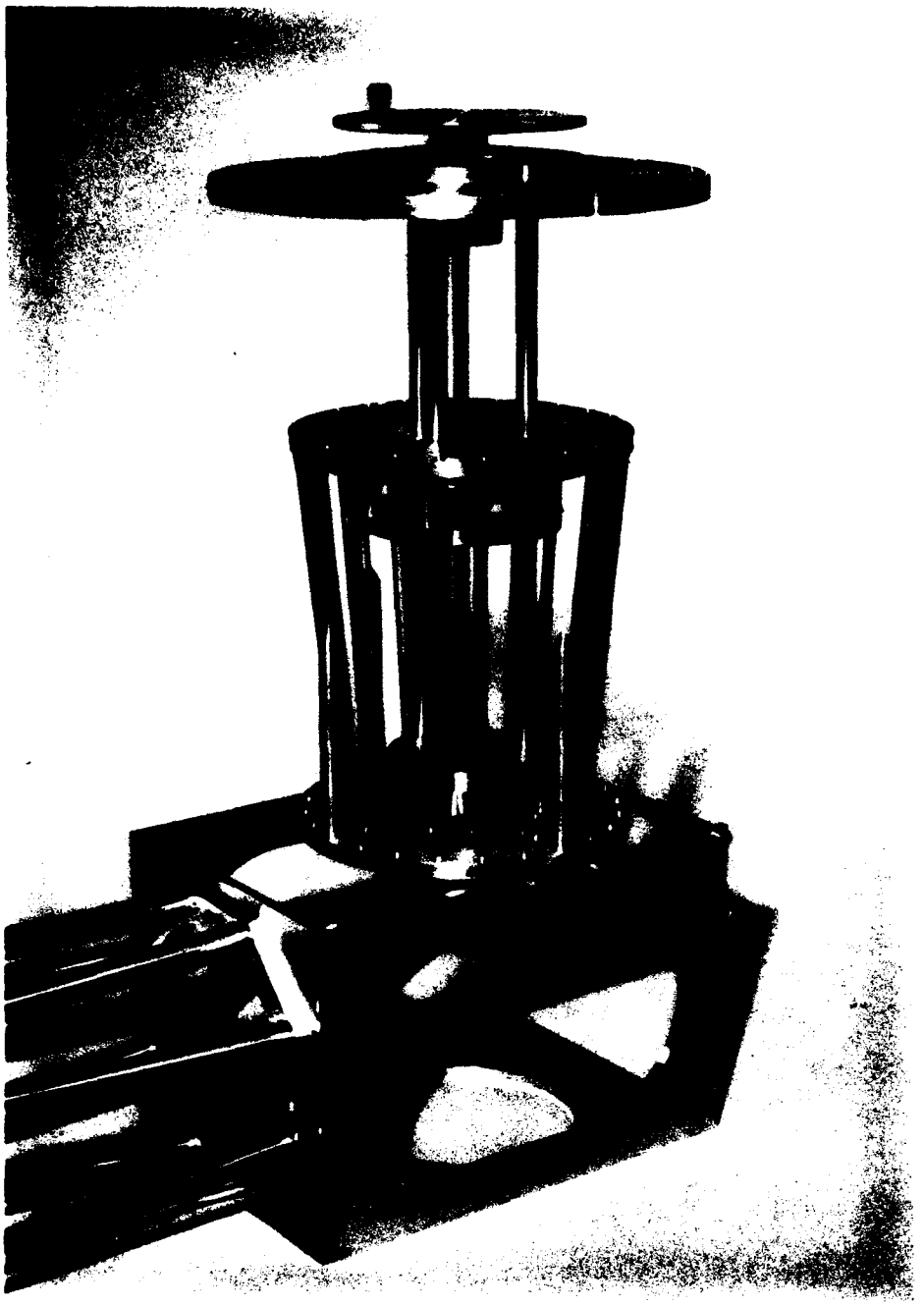

Figure 2-5: Photograph of the frame suspension and vertical positioner.

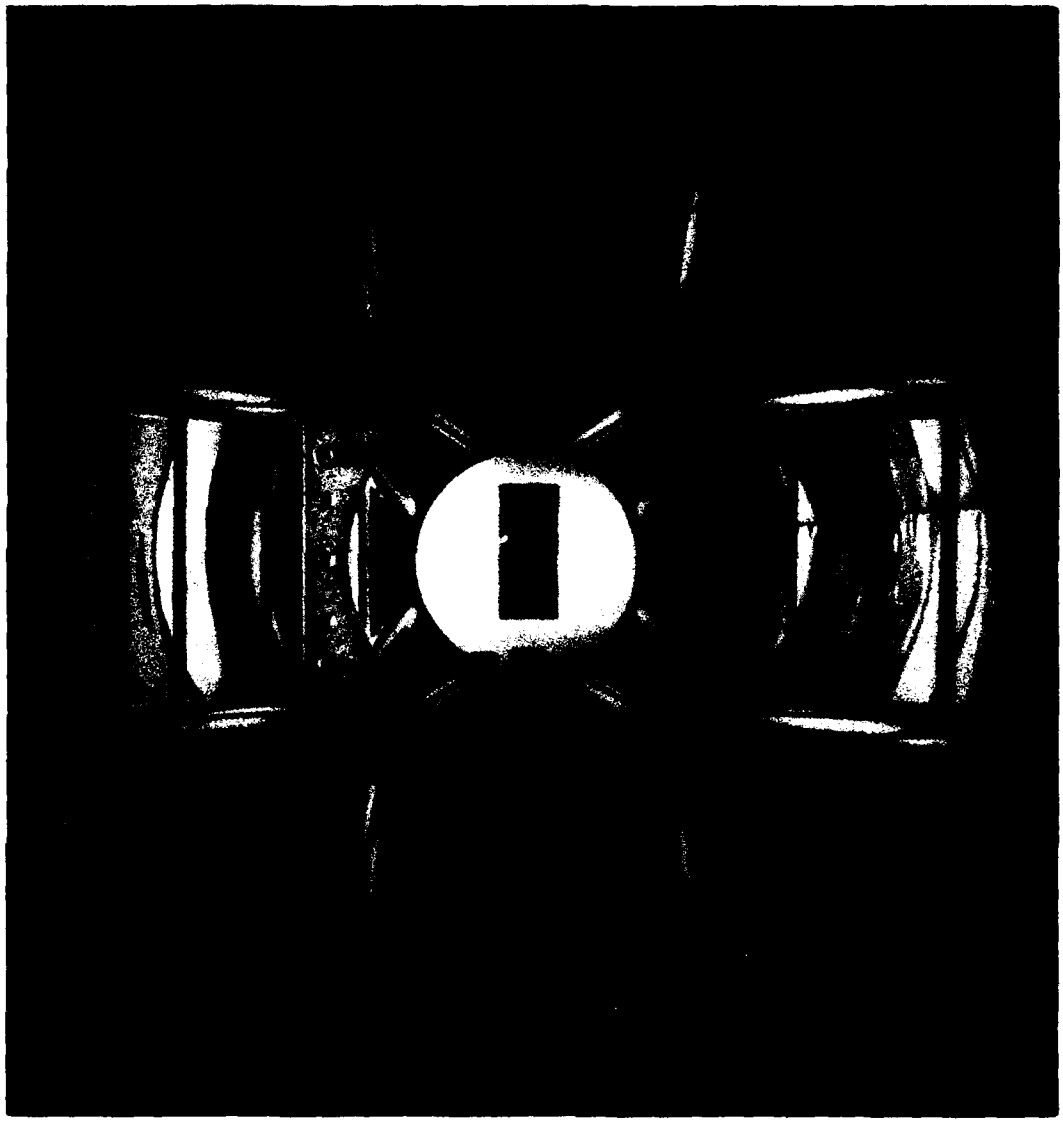

Figure 2-6: Photograph of the reference beam path of the interferometer.

SRL Two-Color Interferometric Plasma Diagnostic

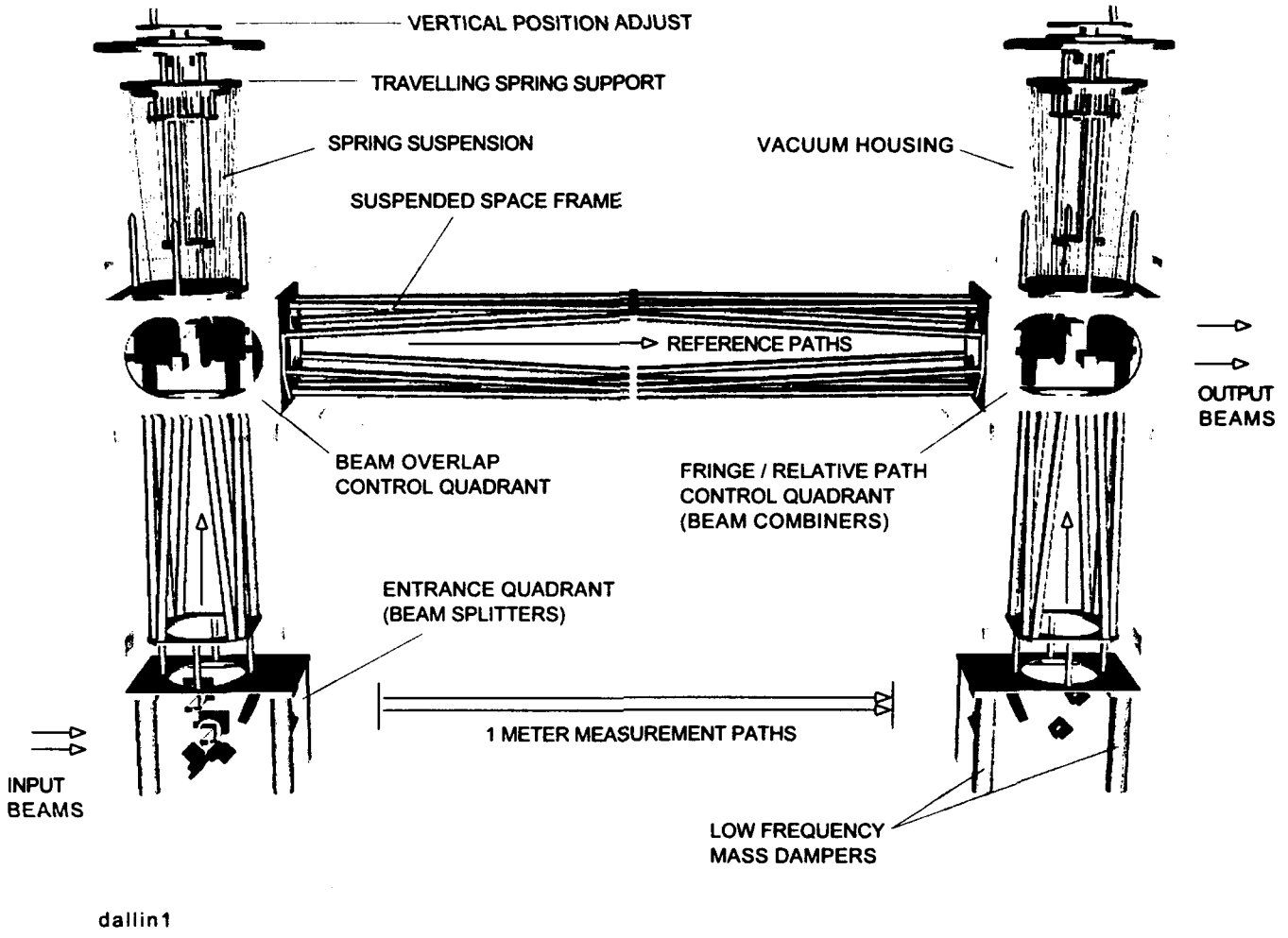

Figure 2-7: Drawing of the interferometer suspended inside the vacuum chamber.

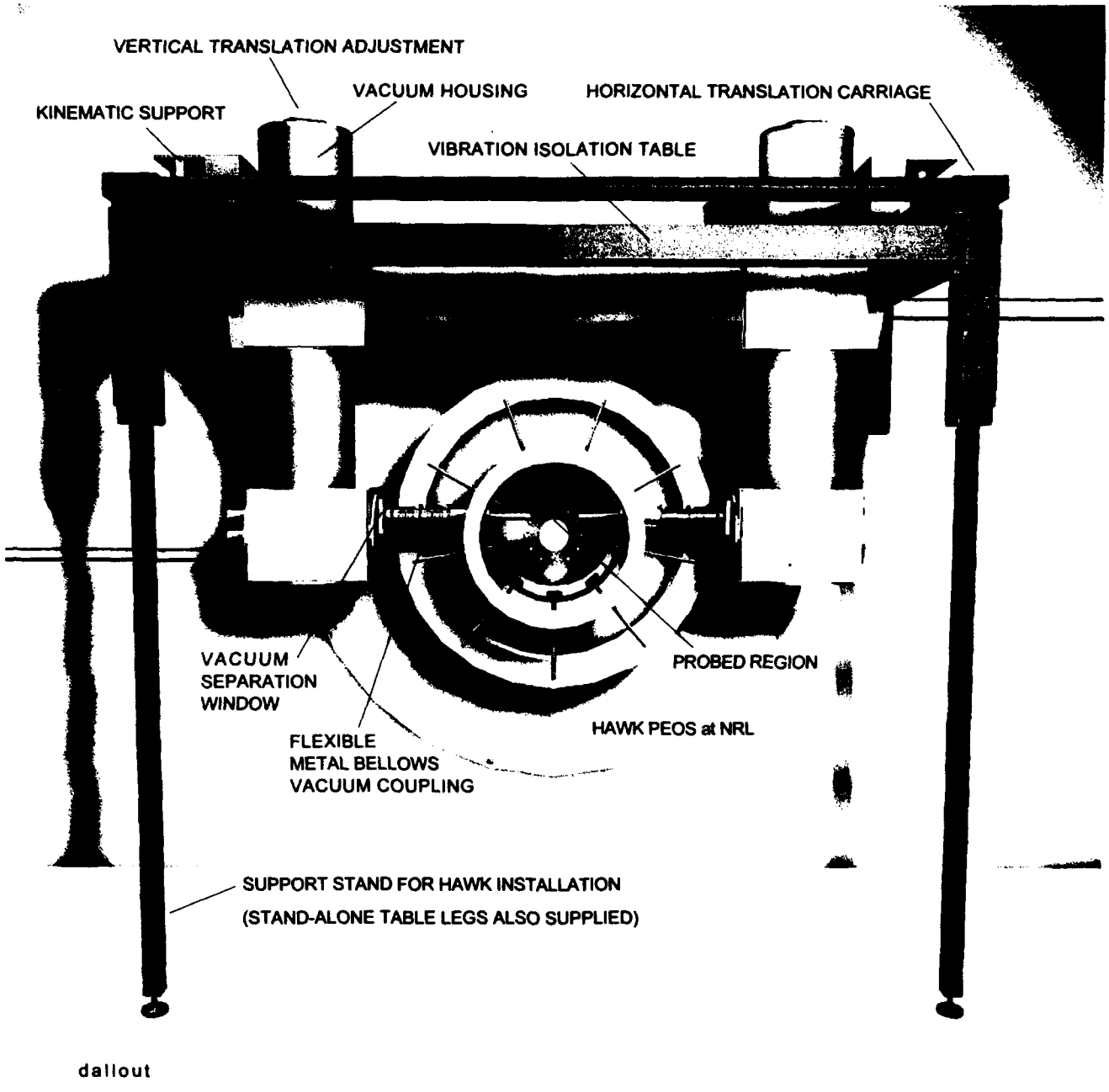

Figure 2-8: Drawing of the interferometer system mounted on the HAWK PEOS.

The spectrum of the noise at high frequencies (near the signals of interest) is discussed later in the section on total instrument noise.

2.5 PROBE LASER OPTICS.

Figure 2-10 shows the optical design of the SRL plasma diagnostic, including the probe laser optics, the interferometer optics and the detection optics.

The probe laser optics are shown at the bottom of Fig. 2-10 and in the photograph of Fig. 2-11. The probe lasers are mounted on a separate table shown in Fig. 2-12, supplied by SRL, which is fixed to the laboratory reference frame. These lasers (only one is shown in the schematic) are Coherent DPSS 532 and DPSS 1064 diode-pumped Nd:YAG systems. The 532 nm laser produces 50 mW. The 1064 nm system produces 100 mW. At the exit window of the lasers are fast, NM Laser Products LST200 mechanical shutters. The original system design was to use 1 watt probe lasers and these shutters were included to prevent excessive heating of the photodiodes. The shutters are not essential at these laser power levels but still have uses to be described in the operations manual. The telescopes expand the laser beams to a diameter of about 1 cm at the exit of the telescopes. The beams converge slowly to a beam waist at the center of the probed plasma and then expand as they move away from the plasma. A pair of lenses outside of the interferometer, also fixed to the laboratory reference frame, act as a variable focus lens allowing the beams to be refocused onto the photodetectors in the screen room some 20 meters away. The spot on the photodetectors is thus a magnified image of the beam waist in the plasma. This arrangement prevents any beam deviation due to plasma density gradients from moving the spots on the photodetectors.

2.6 INTERFEROMETER OPTICS.

The interferometer optics design for the SRL plasma diagnostic are also shown in the center of Fig. 2-10. These optics are fixed to the floating interferometer reference frame. The output

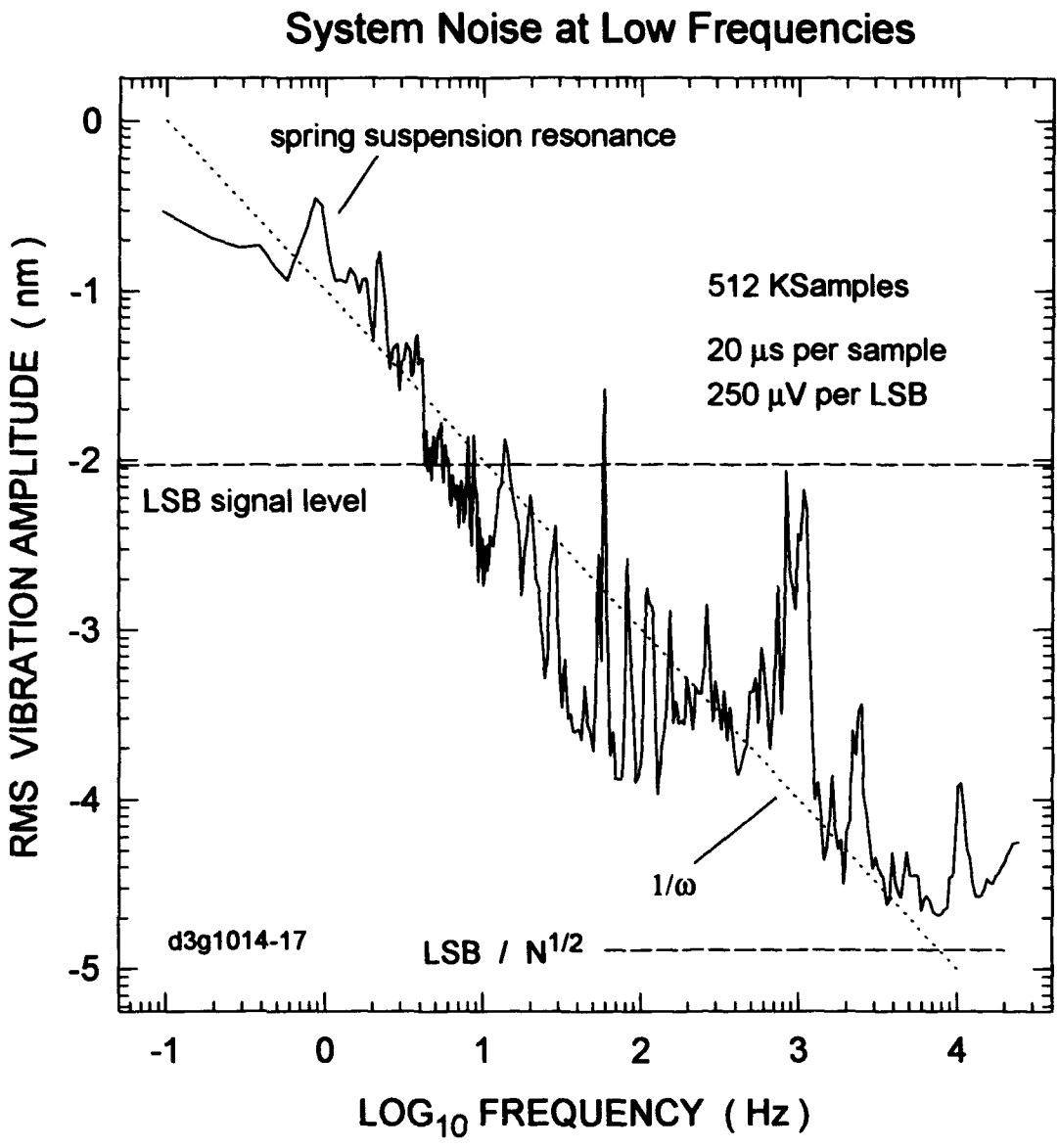

Figure 2-9: Spectrum analysis of the system noise at low frequencies.

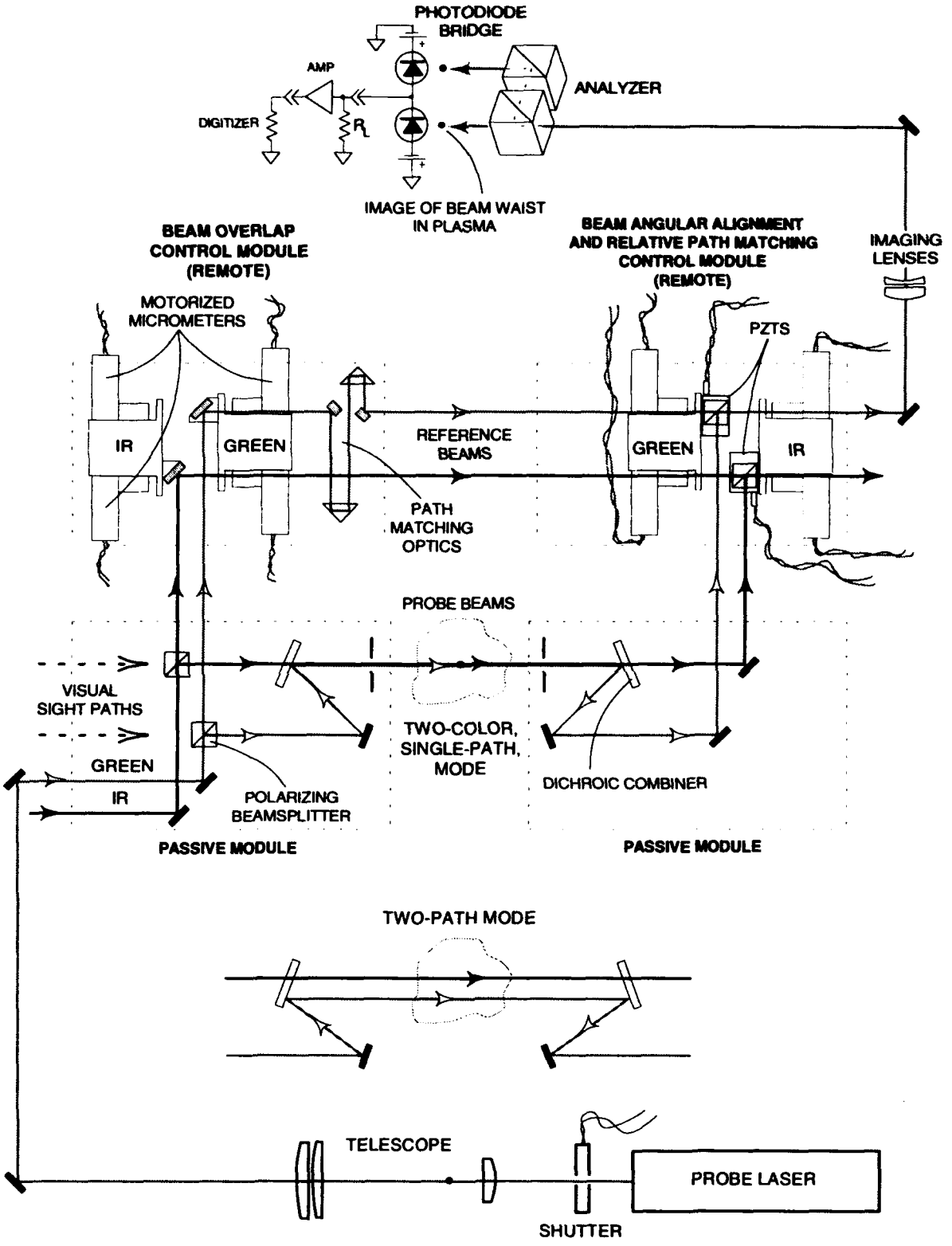

Figure 2-10: Schematic of the optical design for the diagnostic.

Figure 2-11: Photograph of the diode-pumped Nd:YAG probe lasers.

Figure 2-12: Photograph of the probe laser optical table and the interferometer.

beam position and direction is independent of the translation and rotation of the interferometer optics reference frame as long as the input beam and the output beam from the interferometer are parallel and in the same direction. In this design the interferometers for the two wavelengths are totally separate but mounted on the same suspended space frame. The interferometer uses polarizing beamsplitters and combiners as discussed in the Phase I Final Report and the Phase II proposal. The two output beams from each interferometer are thus combined onto a common axis (without interfering) so that they can be passed through normal room air to the analyzer optics where the actual interference occurs. Since the two beams pass through identical air paths, no additional relative path difference is picked up. In the NRL setup, the 532 nm probe beam passed within 1/2 inch of the 60 watt light bulb illuminating the screen room with no ill effects.

A simple dichroic mirror is used to combine the two probe beams by passing the 1064 nm beam and reflecting the 532 nm beam. Tilting these mirrors allows the two probe beams to be placed on a common axis or on parallel axes as shown. The design thus fulfills the SOW requirement that the system be able to probe electron density over two separate paths.

The coherence length of the probe lasers is about 150 m so the interferometers do not have to be path matched for coherence reasons. For optimal sensitivity, however, the reference and scene beams need to be combined at equal distances from the beam waist so that their radii of curvature match (zero fringes over their aperture). The extra jog in the 532 nm beam that the beam combining jog introduces is made up in the upper reference leg of the 532 nm interferometer by the path matching optics shown.

The upper mirrors in the interferometers are mounted on motorized tip/tilt mounts for remote operation. Newport 610 interferometer mounts were modified by replacing the fine control micrometers with Newport 860A-025 motorized micrometers. The modified tip/tilt mounts in the upper left quadrant control the beam overlaps at the polarizing beam combiners. The mirror mounts in the upper right quadrant control the relative tip and tilt of the output beams (allowing adjustment for zero fringes). Generally, the overlap is set once at the beginning of a day's run

and left alone. The interferometer is sufficiently stable that the overlap may not need to be adjusted for several days. The fringes are adjusted more often, perhaps every few hours. The state of the overlap and fringes is monitored by looking at peak signals as the relative paths between the scene and reference beams are swept through several waves (producing a sinusoidal output signal).

The relative paths are adjusted with Burleigh PZS-050 piezoelectric translators (PZT's) between the polarizing beam combiners and the fringe control tip/tilt mounts. These low voltage translators add up to 50 μm of shear to the two output beams which is equivalent to adding a relative path difference between them. The optimal path difference between the reference and scene beams can be achieved by adjusting a DC voltage on these PZT's. Since the drift is about 0.001 waves per second, the system can be left unattended for at least 1 minute before a significant path difference is introduced. An optical fiber feedback loop has been designed and a direct-coupled feedback loop has been delivered to NRL. In practice, they have not been necessary.

2.7 DETECTION OPTICS AND ELECTRONICS.

The detection system consists of the analyzer optics, the photodiode bridges, the signal amplifiers and the digitizing oscilloscope. In the system delivered to NRL the Stanford Research Systems (SRS) SR445 wide-band amplifiers provide gains of 5X, 25X or 125X at a bandwidth of 300 MHz. The LeCroy 7200 oscilloscope with a 2-channel 7242 digitizing plug-in digitizes the signals to 8 bits at 1 GSample/s with a memory depth of 50,000 samples (a total of 50 μs of data). We had hoped to be able to afford a second 7242 plug-in amplifier for the oscilloscope to increase the effective dynamic range of the instrument but, in the end, the budget would not allow it.

The detection optics and electronics are shown at the top of Fig. 2-10. The analyzer consists of two polarizing beamsplitters rotated around the axis of the incoming beams by 45°.

The first polarizer picks off half of the scene beam and half of the reference beam and combines them onto a single axis at 90° to the incoming beams. These beams can now interfere. The other halves of the reference and scene beams pass through the first polarizing beamsplitter and interfere on the lower photodiode. The deviated beams are reflected off of a second polarizing beamsplitter to direct them onto the second photodiode and increase the fringe contrast.

Several types of photodiodes are used in the detection bridges, depending on the wavelength being detected and the size of the photodiode required. Two bridge circuits were built using EG&G FFD-200 photodiodes which have a fast risetime of 2 ns into 50 Ω and an active area of 20 mm^2. These photodiodes work well at 532 nm where they have a responsivity of 0.33 amps/watt. They proved to be a bit small for the larger diffraction spot sizes of the 1064 nm beam, however, so a bridge was built for the IR probe with EG&G YAG-444 photodiodes. These photodiodes are optimized for 1064 nm where they have a responsivity of 0.7 amps/watt. Even though they have an active area of 100 mm^2 (11 mm diameter) their specified risetime is 5 ns with a 180 V reverse bias. In the NRL experiments, however, the reverse bias used was only 90 V so the risetime was only 10 ns.

The larger photodiodes make it easier to collect all of the light from the probe beams. These beams exhibit a positional jitter of 1 to 2 mm due to air currents and vibrations in the beam steering mirrors. Beam excursions off of the photodetectors can lead to low frequency differential signals so they should be well contained.

Large or small, it would be best if the two probes used the same size photodiodes. The signals are subtracted from each other in the analysis and differences in risetimes can lead to analysis error (as we will see below). EG&G SGD-444 photodiodes (the equivalents of the YAG-444 but optimized for the visible) were supplied to NRL but were not mounted in a bridge circuit. For faster risetimes, NRL should purchase EG&G YAG-200 photodiodes to match the FFD-200 photodiodes used in the 532 nm bridge.

The differential photodiode bridge signal is either fed directly to the digitizing oscilloscope or to a wide-bandwidth amplifier, depending on the size of the signal expected. Typically the load resistor, R_L, is 50 Ω. The output signal from the bridge is determined by the power in the probe lasers, the sensitivity of the photodiodes, the losses in the optical train and the relative alignment of the two output beams from the interferometer (the fringes). In the initial NRL experiments the peak-to-peak variation in the 532 nm signal is 0.6 V, as the relative path in the interferometer is swept over a wave. The point of maximum sensitivity occurs at a differential voltage of zero where the response is linear with a sensitivity of $\pi \times 0.6$ V or about 2 V/wave. The 1064 nm laser is more powerful and its photodetectors are more sensitive so its typical peak-to-peak signal was about 2 V for a sensitivity of about 6 V/wave at the zero crossing. No further amplification was required (or desired) for measurements of the electron and neutral densities in a full shot through the HAWK plasma. Amplification of 5X, 25X or 125X were possible for more sensitive measurements.

2.8 INSTRUMENT NOISE.

The noise level of the SRL plasma diagnostic as delivered to NRL is generally limited by shot noise on the photodiode current for time scales of less than 1 microsecond. This is at true, at least, if the signals (i.e. the electron densities) are low enough for the SRS wide-bandwidth amplifiers to be used. In practice, the photodiode bridge signals in the NRL tests were often digitized directly by the Lecroy 7200 oscilloscope rather than being amplified. This was because the SRS wide-bandwidth amplifiers clip their output signal at a maximum of 1.5 volts (0.3 V at the input of a 5X gain stage). This maximum input level was often exceeded when large plasma densities were being measured. The Lecroy input amplifiers proved to be considerably noisier than the fixed-gain, wide-bandwidth amplifiers and thus were generally the limiting factor when measuring high density plasmas.

Since both shot noise and thermal noise are random processes their levels are proportional to the square root of the measurement bandwidth, B, and are generally specified in terms of nV/$\sqrt{\text{Hz}}$. The rms voltage on a load resistor, R, due to shot noise on a current, I, is given by $R\sqrt{2eIB}$ where e is the charge on an electron (1.6×10^{-19} coulombs). The voltages measured on the photodiode bridges indicate that about 20 mA is flowing through each photodiode in the 1064 nm bridge and about 6 mA is flowing through the 532 nm bridge. The noise voltage on the 1064 nm bridge difference signal (add another $\sqrt{2}$ for differencing) with a 50Ω load should thus be about 6 nV/$\sqrt{\text{Hz}}$. For the 532 probe the noise is smaller by a factor of 2 at about 3 nV/$\sqrt{\text{Hz}}$. Note, however, that the 532 nm SIGNAL is smaller by a factor of 3 so the 1064 nm S/N is better).

The rms thermal noise voltage on the load resistor is given by $\sqrt{4kTBR}$ where k is Boltzman's constant (1.38×10^{-23} J °K^{-1}). This evaluates to 0.9 nV $\sqrt{\text{Hz}}$ for a 50 Ω load at room temperature (T=300°K). The new SRS wide-band amplifiers purchased for NRL are specified to have an input noise voltage of 2.2 nV/$\sqrt{\text{Hz}}$ (the old specification used in the proposal was 1.1 nV/$\sqrt{\text{Hz}}$). This noise level is just below the noise levels expected from the shot noise.

The noise specification on the LeCroy oscilloscope amplifiers provided by their engineers at the time of the proposal was 170 μV rms or 10 nV/$\sqrt{\text{Hz}}$ (given their 300 MHz bandwidth). The noise actually measured on the amplifiers purchased for NRL, however, was 750 μV or about 40 nV/$\sqrt{\text{Hz}}$. This means that the fluctuations observed on the high electron density signal in the following section (where the amplifiers were not used) are due to oscilloscope noise. The shot noise fluctuations on the photodiode bridge signal must be amplified by at least two stages of the lower-noise, wide-band amplifiers (a total of 25X) before they are larger than the noise on the oscilloscope amplifiers. This amplification will only be possible for the measurement of very small electron densities where the resulting signal would not be clipped by the wide-band amplifiers.

The discussion above makes the assumption that all of the electronics noise sources in the detection circuits and all of the photon noise sources in the probe laser beams are truly random. A spectrum analysis of the output signals from the detection electronics both with and without the probe beam power on the photodiodes shows that this is not entirely the case. Figure 2-13 shows these spectral analyses for both the 1064 nm probe and the 532 nm probe. The data traces taken without the probe beams on the photodiodes (i.e. without shot noise on the signal) were taken with the Lecroy input amplifiers at its maximum gain of 40 mV full scale and with two stages of gain (25X) on the SRS wide-band preamplifiers. The data traces with the probe beams on the photodiodes were taken with less gain (80 mV full scale) on the Lecroy input amplifiers (and thus somewhat less noise).

The high frequency noise spectra in Fig. 2-13 show that the measured noise in the detection circuits alone rises for frequencies below 1 MHz. Above about 45 MHz the measured noise rolls off due to the 5.5 ns RC time constant of the photodiode junction capacitance. The photodiode current in the presence of the probe lasers was measured by adjusting the path difference in the interferometer to swing the probe beam first into one of the photodiodes in the bridge and then into the other. The shot noise spectrum estimated for the measured photodiode current, shown as a dashed line in the two figures, is flat below the 45 MHz rolloff frequency. Generally, the graphs show that above 1 Mhz the electronics noise and the shot noise are roughly equivalent. The 1064 nm probe is closer to the optimum since it has twice the laser power and the photodiodes are better matched to the probe wavelength. Below 1 MHz the 532 nm probe laser shows less noise because it is controlled by an etalon to be single mode. The 1064 nm probe laser shows some residual mode beats at about 260 kHz (this has since been rectified by replacing the 1064 nm probe laser used in these tests with a single mode unit containing the required etalon). The longitudinal mode beats result in an intensity fluctuation which is not fully eliminated from the difference signal unless the system is exactly at the 1/4 wave condition that balances the photodiode signals. This beat can be seen in the baselines of some of the data sets taken on HAWK plasmas.

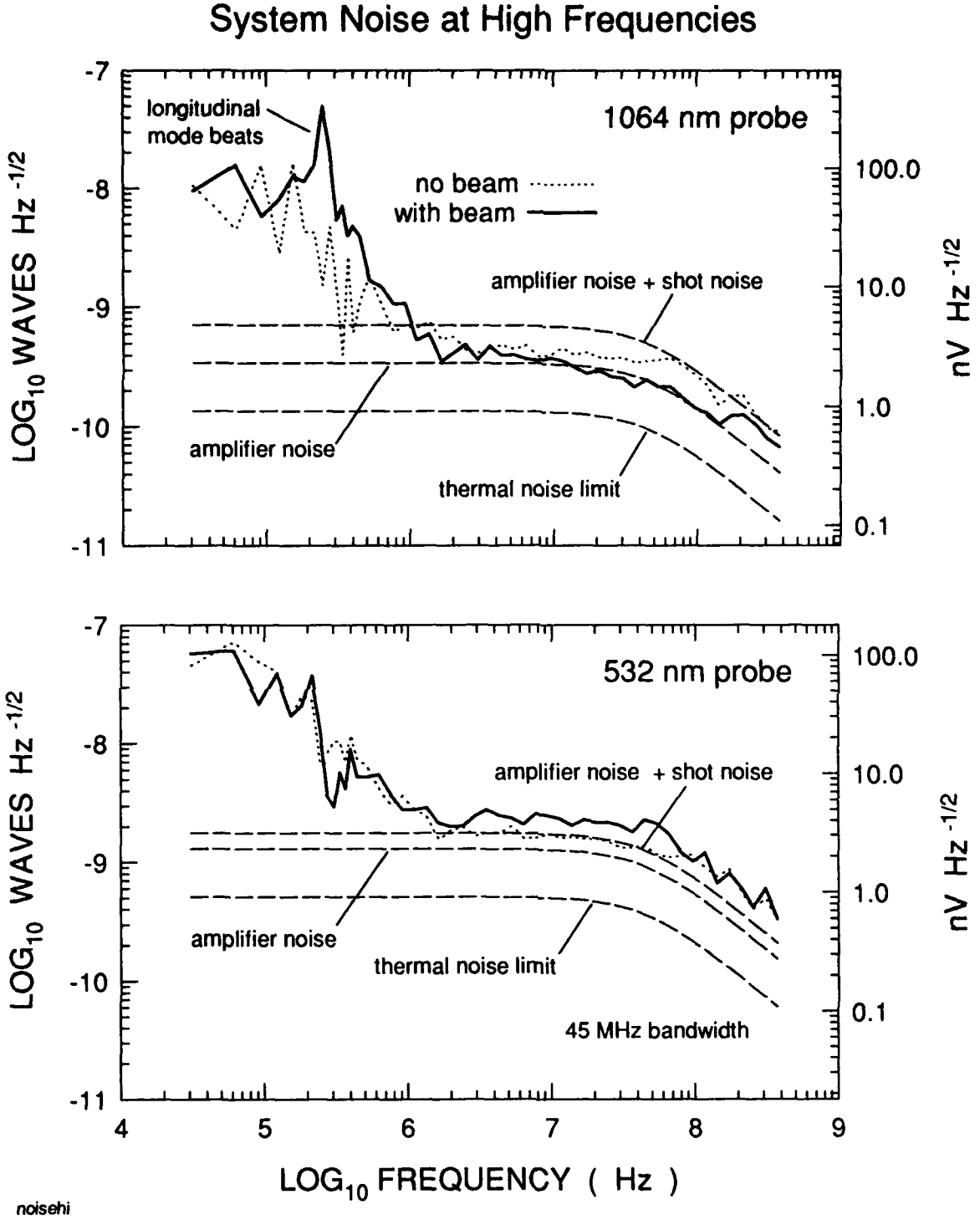

Figure 2-13: Spectrum analysis of the total system noise at high frequencies.

Finally, note that the noise on the neutral species density as determined from the analysis is greater than the noise on the electron density. This is because the signal due to neutrals is 50X smaller than the signal due to electrons. For cleaner measurements of the neutral density the power in the probe lasers would have to be increased.

2.9 MODIFICATIONS SUGGESTED FOR LARGE SIGNALS.

The design of the SRL plasma diagnostic minimizes the effects of intensity noise on the probe lasers by the use of differential detection. A phase shift causes the signal from one photodiode to rise and the signal from the other to fall. When the relative path difference in the interferometer is $\lambda/4$ the power of the probe laser is equally divided between the photodiodes and the bridge signal is zero. In this situation the bridge cancels out fluctuations on the probe laser intensity since these fluctuation cause the photodiode signals to rise and fall together. Probe laser intensity fluctuations are typically 0.1% to 0.5% which is much larger than the shot noise or thermal noise signal described above. This bridge condition is also the point at which the system is most sensitive since the signal voltage is proportional to $sin(\delta\phi)$.

When the bridge is not closely balanced, more power from the probe falls on one photodiode than on the other. Fluctuations on the laser power are then not fully canceled. Electron densities in the HAWK experiments at the time the switch opens result in a fringe shift of about 1/4 wave. The bridge was often deliberately offset to -1/8 wave before a shot to maximize the system linearity and sensitivity at the electron densities of interest (an excellent suggestion from Bruce Weber). This means, however, that over much of the signal, particularly in the offset baseline before t=0, the laser power fluctuations are not fully canceled by the bridge.

The power fluctuations in the 532 nm probe laser are relatively small since it is designed to run on a single longitudinal resonator mode. The 1064 nm probe laser, however, will occasionally jump between longitudinal modes and, at these times, there is a significant beat signal in its output

intensity. If the output intensity of the probe lasers were recorded, then the signal voltage could be normalized to correct for these fluctuations.

The suggested modifications are thus (1) replace the current 1064 nm probe laser with its single-mode version (a cost of about 4K$ if done immediately) and (2) acquire a second LeCroy 7242 plug-in to record the probe laser intensities (a cost of about 13K$). The second plug-in could also be used to increase the system's dynamic range as initially intended. (Note in proof: Both of these modifications have since been completed.)

SECTION 3

MEASUREMENTS ON THE HAWK PEOS AT NRL

3.1 OVERVIEW.

The following figures show the essential results of the measurements made on the HAWK PEOS at NRL. Most of the measurements shown here were taken by both SRL and NRL personnel as the diagnostic was being set up and tested. Later, NRL personnel took additional data in a different region of the switch.

The SRL/NRL tests began with shots in which only the flashboards were fired. These measurements are essentially what SRL would have performed during the planned flashboard tests at the SRL facility. The flashboard tests were followed by tests in which the Marx bank of HAWK was fired, both with and without the flashboards being fired. The above tests were completed during the three weeks and served both to test the instrument and to instruct NRL personnel in its operation. The original data sets of all of the shots and photocopies of the lab notebook pages describing them were transferred to NRL before the SRL personnel left.

Figure 2-8 shows the flashboard and probe path arrangement used in the SRL/NRL acceptance tests. The probe volume chosen was a chord through the plasma between the center conductor and the ring of rods (the cage) which form the outer conductor. The path length was 16.4 cm in length and 1.4 cm above the top surface of the center conductor. Only 9 flashboards were used in these tests rather than the 18 usually used. This arrangement provided for simpler access to the probed volume while maintaining a cylindrical symmetry of flashboards. The tubes shown extending into the HAWK vacuum chamber and resting on the outer rod cage of the PEOS serve to shield the probe beam from flashboard plasma outside of the switch volume.

The interferometer vacuum housing was connected to the HAWK vacuum housing with flexible metal bellows to minimize the coupling of room vibrations into the interferometer. The two vacuum regions were separated, however, by windows on the vacuum housing. The SRL plasma diagnostic can be operated with only a minimal vacuum on the order of 0.1 Torr. The HAWK PEOS needs a pressure of better than 10^{-4} Torr.

NRL continued experiments on HAWK on their own during the few remaining weeks of FY93. This work included moving the interferometer probe beam down the axis of the HAWK PEOS by some 25 cm to a region where the electron density was too low to be measured with the original heterodyne interferometer. Dr. Bruce Weber has sent some of the results of these tests to SRL for inclusion in this Final Report.

3.2 NOISE LEVEL TESTS.

We begin with the data taken by Dr. Weber at NRL since it directly addresses the maximum sensitivity of the SRL plasma diagnostic using the probe lasers, photodiodes and electronics delivered to NRL. This data, shown in Fig. 3-1, includes the total generator current from the Marx bank, the current in the short circuit load and the electron density as determined by the SRL plasma diagnostic. The electron density signal is deliberately magnified to best illustrate its noise level.

The noise on the electron density trace before about 0.6 μs is due to the combination of the shot noise on the photodiode current and the thermal noise in the wide-band amplifier. The amplifier was set for a gain of 25X in this case. The larger, high frequency ringing seen on the baseline from about 0.8 μs to the steep rise in the electron density signal is radiated noise leaking into the screen room. This type of noise was seen on data shots in which the lasers were blocked. The noise is real, of course, but could be reduced by patching some of the holes in the screen room and/or adding more filters to its internal 120V AC power. Alternately, an FFT of the signal could be filtered to remove a narrow band around the ringing frequency of this noise.

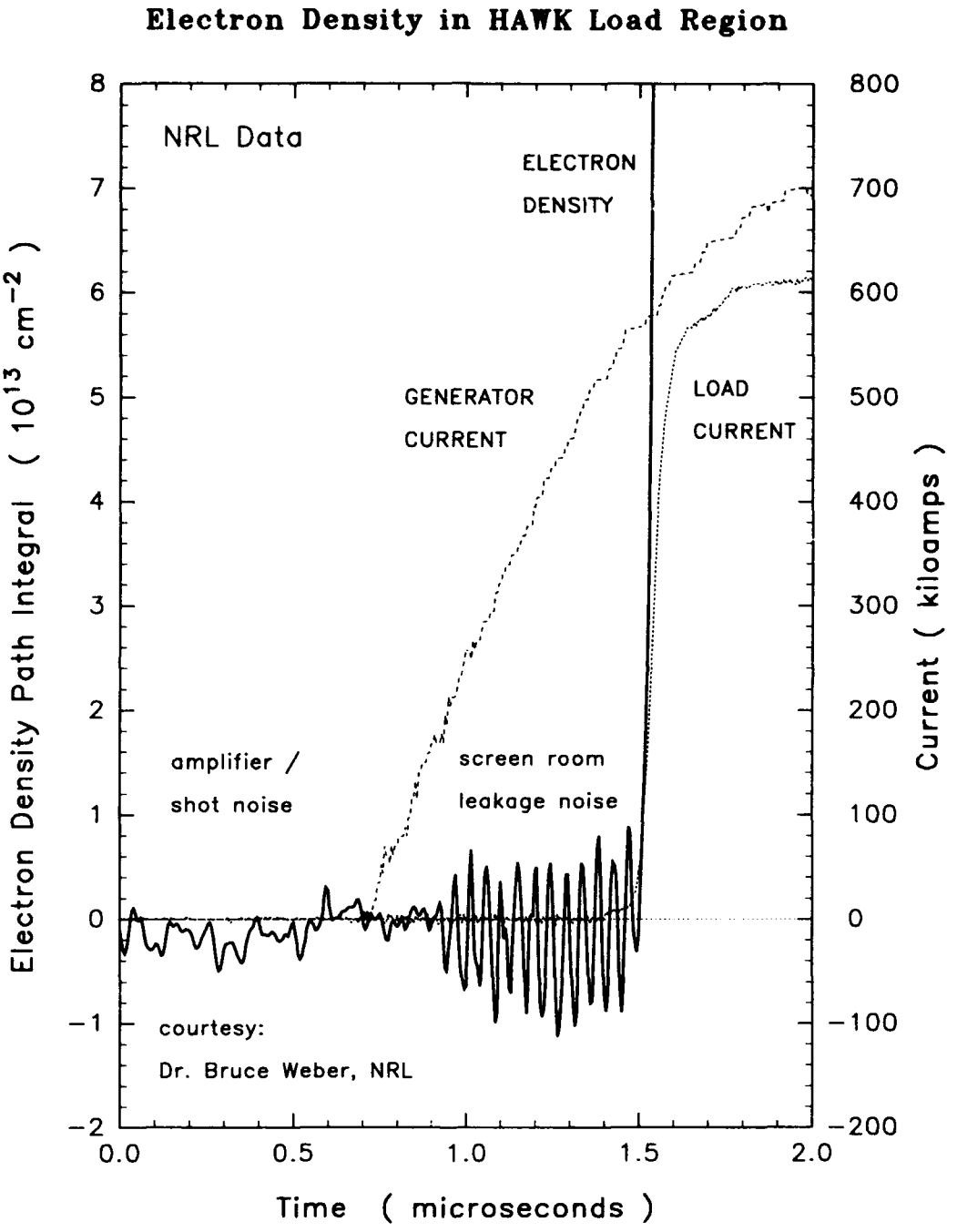

Figure 3-1: Measurement by NRL in the load region of the HAWK PEOS.

The rms noise due to the shot and thermal noise is roughly 3×10^{12} cm^{-2} in electron density units. Since the 1064 nm probe is most sensitive to electron density we can assume the noise is primarily on that probe. At the 1064 nm wavelength this electron density corresponds to a fringe shift of 1.5×10^{-5} waves.

The data points shown are an average of five 1 ns samples, corresponding to a bandwidth of about 60 MHz. As described above, the shot noise on the 1064 nm probe was expected to be about 6 $nV/\sqrt{Hz}$, or 50 μV at 60 MHz. The 1064 nm bridge circuit typically had a peak-to-peak swing of 2 V which is equivalent to a sensitivity of about 6 V/wave for small signals. The 50 μV of noise thus corresponds to a fringe shift noise of about 8×10^{-6} waves or about half of the observed noise.

The oscilloscope should not have contributed much to this noise. A 50 μV noise, amplified by a factor of 150 is 7.5 mV which is well above the oscilloscope amplifier noise of 750 μV. Assuming that the oscilloscope was set at 20 mV/division (160 mV full scale) the least significant bit (LSB) would be 625 μV so digitization noise in not significant.

The agreement with the expected noise levels is not too bad, considering that there are other sources of noise which are not fully accounted for above. The fringe contrast at the photodiodes, for instance, is undoubtedly not 100%. There is thus some laser power on both photodiodes which does not contribute to the signal but which does contribute to the shot noise. A better assessment of the noise levels would require additional measurements.

3.3 HAWK FLASHBOARD TESTS.

Figure 3-2 shows the results of a measurement of the plasma produced in the switch volume by firing all 9 of the flashboards but not the HAWK Marx bank. The top graph shows the result of analyzing both probe signals as being the result of only an electron density. This is equivalent to all of the electron density measurements performed previously on this switch. The electron density begins to ramp up before t=0 because the flashboards are fired 1.5μs before the

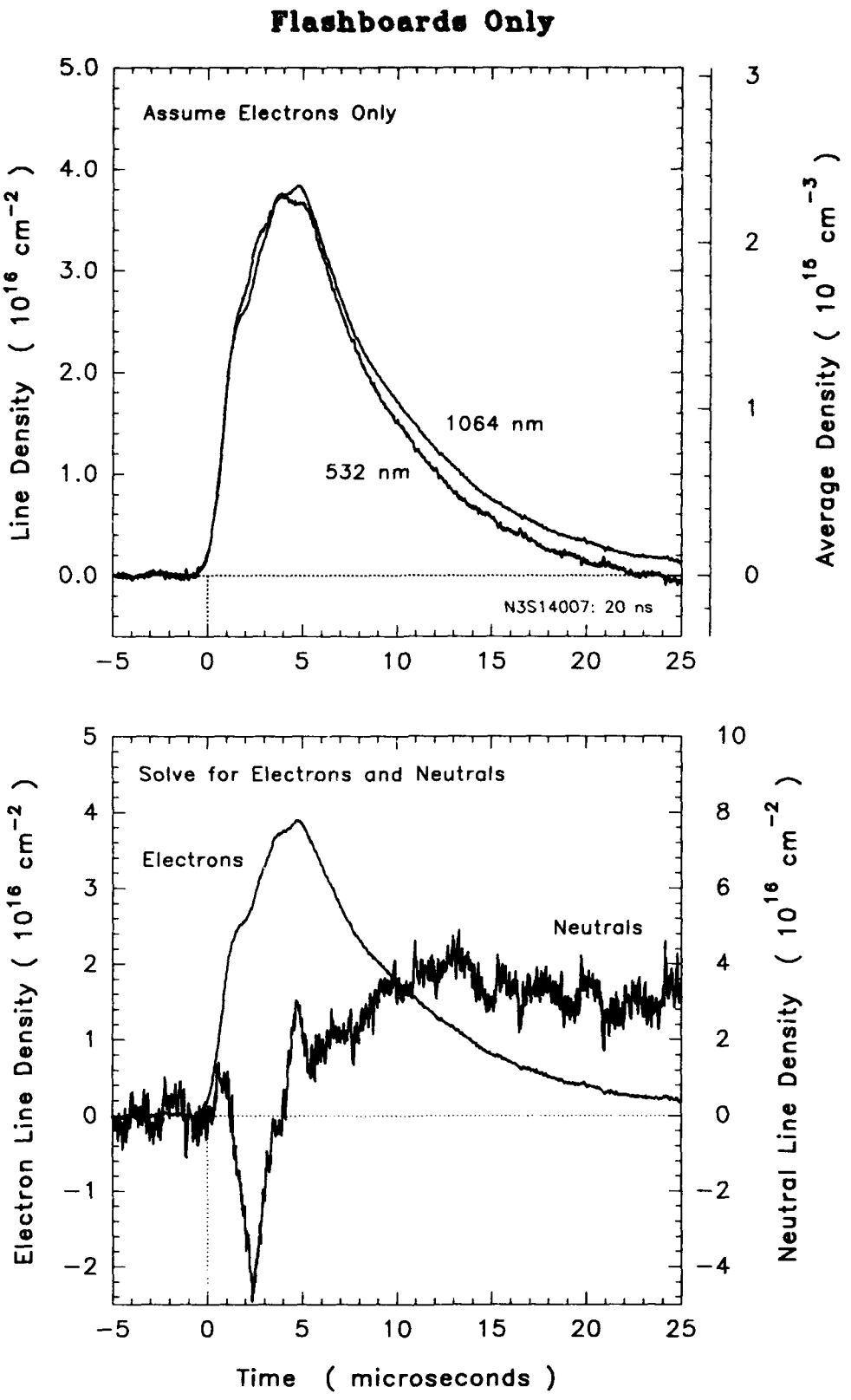

Figure 3-2: Measurement of the plasma produced in the HAWK switch region by 9 flashboards.

oscilloscope (which is triggered on the Marx bank trigger). The measured electron densities of 2×10^{15} cm^{-3} and the general temporal profile agree well with the densities measured previously with the heterodyne interferometers. These densities were also typical of those measured above the Maxwell flashboards in Phase I of this program. The actual data set covers a full 50 μs with a data point every 1 ns. The data was averaged over a 20 ns window to reduce the file size and reduce the noise on the traces.

Features on the upper traces to note are the fact that at later times the 532 nm trace falls below the 1064 nm trace. This is because the 532 nm probe is more sensitive to the positive refractive index of the neutrals than the 1064 nm probe which causes the curve to shift downwards in this plot. It is the difference between these two curves that determines the density of the neutrals. Note that the 532 nm probe trace drops below the baseline towards the end of the graph. This would be unphysical if there were only electrons in the plasma (and thus shows up as a negative electron density in this analysis which assumes only electrons).

Another feature of this data set is that in the rising portion of these traces the electron density predicted from the 1.064 nm probe drops below the electron density predicted from the 532 nm probe. This could not occur in a plasma consisting of only neutrals and electrons. The cause of this effect has not been definitely determined, but numerous experiments were performed to test several possibilities. The most likely cause, as discussed in Section 2.3, is that an excited state of a neutral species is formed which has an absorption line between 532 nm and 1064 nm.

The lower graph of Fig. 3-2 shows the results of an analysis in which both electrons and neutrals are assumed to exist in the plasma. The resulting trace for the neutrals is relatively noisy because the probes are about 40 times less sensitive to neutrals than to electrons. The result of the excursion of the 1064 nm probe trace below the 532 nm probe trace, whatever its physical origin, causes the analysis to report an unphysical negative neutral density. This occurs

at a bad time, unfortunately, since the neutral density in the rising portion of this trace is the quantity of interest in predicting how the opening switch will perform.

An indication of the accuracy of the data is given by the graphs in Fig. 3-3 in which the natural logarithms of the electron and neutral densities are plotted for the time period after the electron density has peaked. The decrease in the electron density is very close to a pure exponential decay with a characteristic time of 7 μs and is followed for about four e-folds (to about 2% of its starting value). Note that the neutral density, on the other hand, increases for about 10 μs and then stays constant as would be expected. The neutrals are coming from the flashboards around the perimeter of the chamber and are being driven in. There is no place for them to decay away to on these time scales.

Figure 3-4 shows the result of a flashboard test in which only one flashboard was fired on the opposite side of the chamber from the probe beam. The flashboard fired was actually 40 degrees from bottom dead center so the probe beam volume was illuminated by the ultraviolet light from the discharge on the flashboard. The rise in the electron density is delayed by about 7 μs due to the added distance from the flashboard to the probed volume. Electrons and neutrals, however, are formed at t=0 in the probed volume, probably as a result of the UV light emission from the flashboard. The peak electron density is lower by a factor of 6 and both probe traces, when analyzed only as electrons, drop below the baseline. When analyzed as both electrons and neutrals the electron density drops back to zero as it should and the neutral density builds up towards a constant value. The drop in the neutral density near the peak of the electron density could be either the result of the excited states as suggested earlier or the fact that the density of neutrals created in the center of the chamber (by the UV?) would decay rapidly as they spread out into the vacuum chamber.

Other flashboard data shots taken may contain other useful information, but these traces suffice to indicate how the SRL plasma diagnostic performs in these situations.

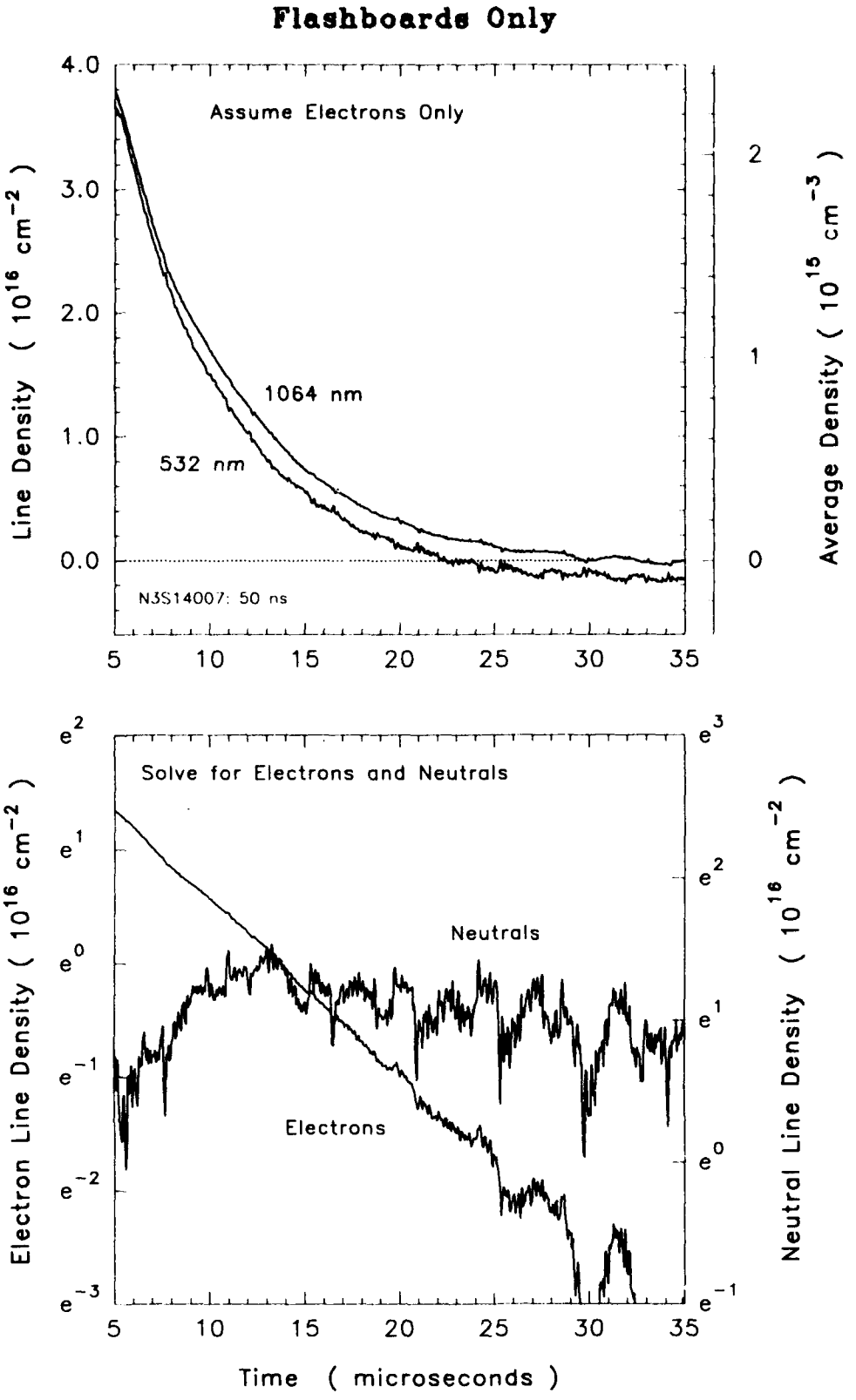

Figure 3-3: Exponential decay of the electron density in the HAWK flashboard plasma.

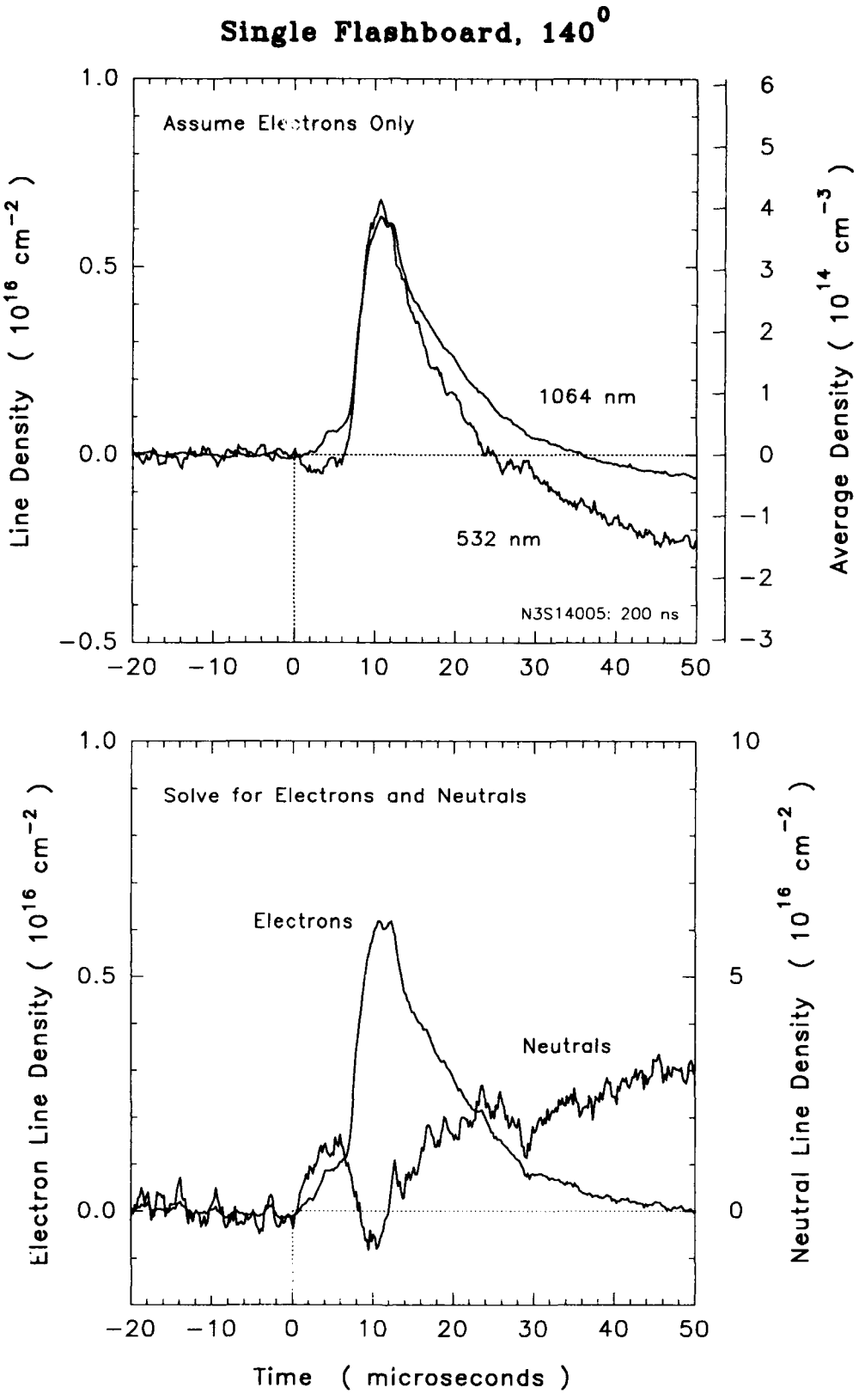

Figure 3-4: Measurement of the electron density from one HAWK flashboard opposite the side of the probed region.

3.4 HAWK PEOS TESTS.

Figure 3-5 shows the results of a probe of the switch volume in which the Marx bank is fired but the flashboards are not. Such shots are taken at NRL to test the current diagnostics. In the upper traces the two probes are analyzed assuming there are only neutrals present. The directional convention on the graph is not reversed, however, so the traces still move downwards to indicate the presence of neutrals. Note that the electron density in the switch volume is very low compared to the neutral density in this shot. The neutrals are coming from the center conductors since their density increases at first and then drops as they expand out into the vacuum chamber.

Figure 3-6 shows the data taken during a full shot of the HAWK PEOS, including all of the flashboards and the Marx bank. Note that both the 1064 nm probe and the 532 nm probe, analyzed as electrons, track upwards close together for the first 1.2 μs. At that point the "snowplow" increase in electron density occurs before the electron density plummets as the switch opens. When analyzed as electrons and neutrals the data indicates a sharp, anomalous, negative spike in the neutral density (discussed below) at the time the switch opens. Immediately after opening, however, the neutral density begins to rise very rapidly and is typically an order of magnitude greater than the electron density.

Figure 3-7 shows an expanded portion of the data set around the time that the switch opens. At 1.34 μs the 1064 nm probe trace (analyzed as electrons) begins to drop and the 532 nm probe trace begins to rise. Both effects could possibly be due to the production of an excited state with an absorption line between the two wavelengths as discussed in Section 2.3. The 1064 nm probe trace continues to drop and the 532 probe trace peaks and drops rapidly some 20 ns later. It is highly unlikely that more than a few nanoseconds of this apparent 20 ns delay could be accounted for by electronics or different optical path lengths back to the screen room. The

rapid switching indicated by the 532 nm probe (while showing off the bandwidth of the system nicely) could be partially due to the rapid decay of the (as yet hypothetical) excited state.

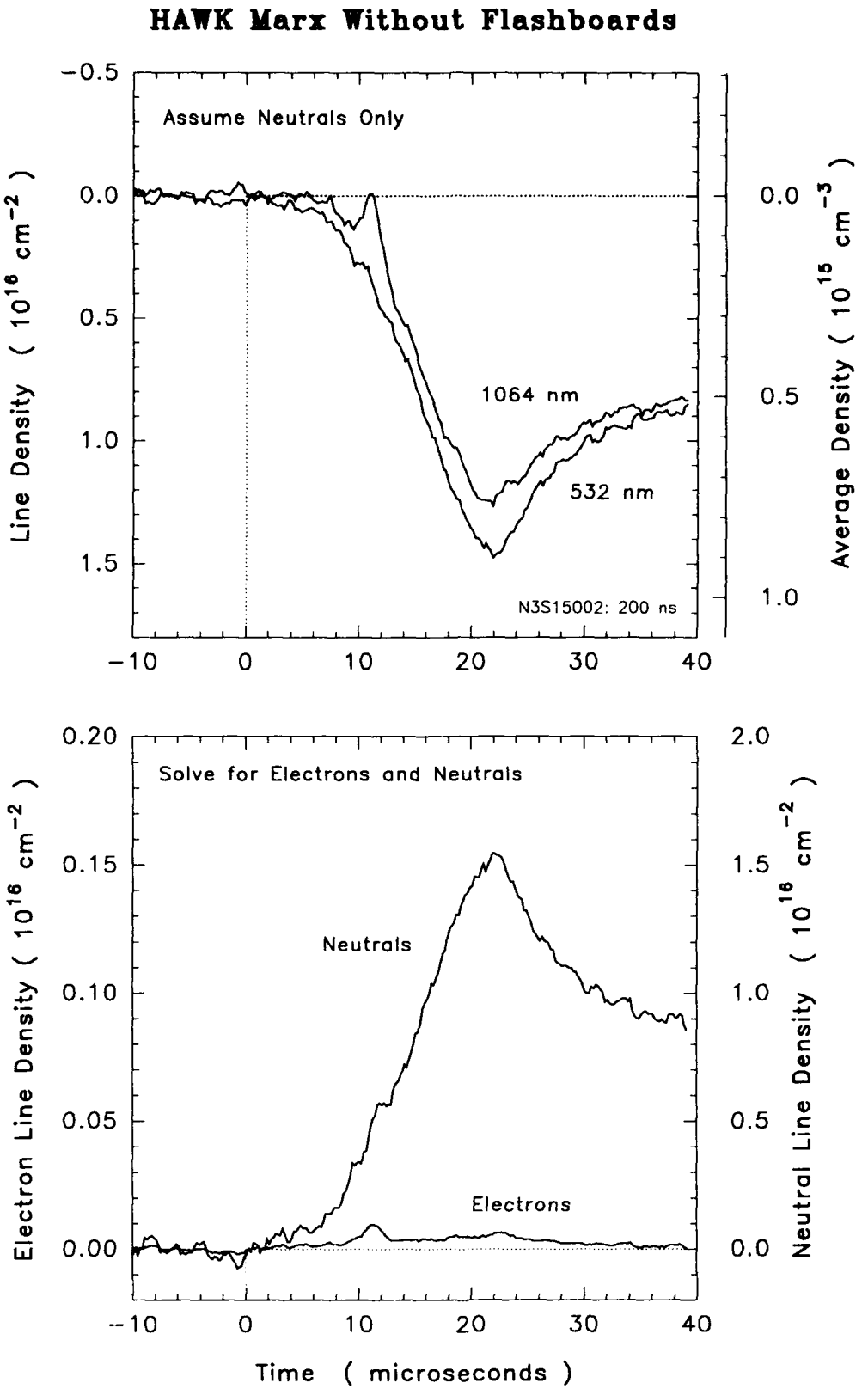

Figure 3-5: Measurement of the neutral density produced by the HAWK generator current in the absence of the flashboard plasma.

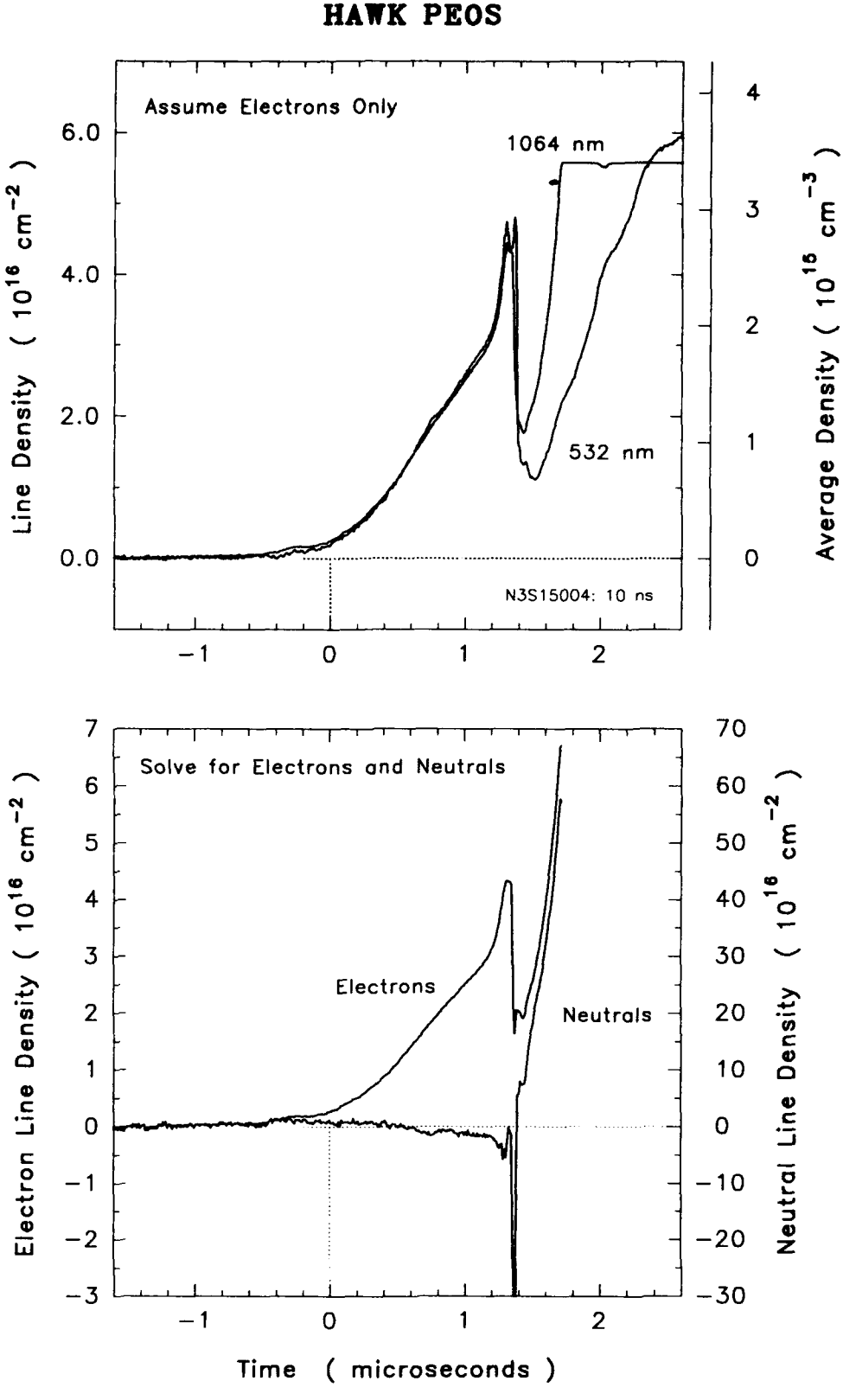

Figure 3-6: Measurement of the plasma in a full HAWK shot.

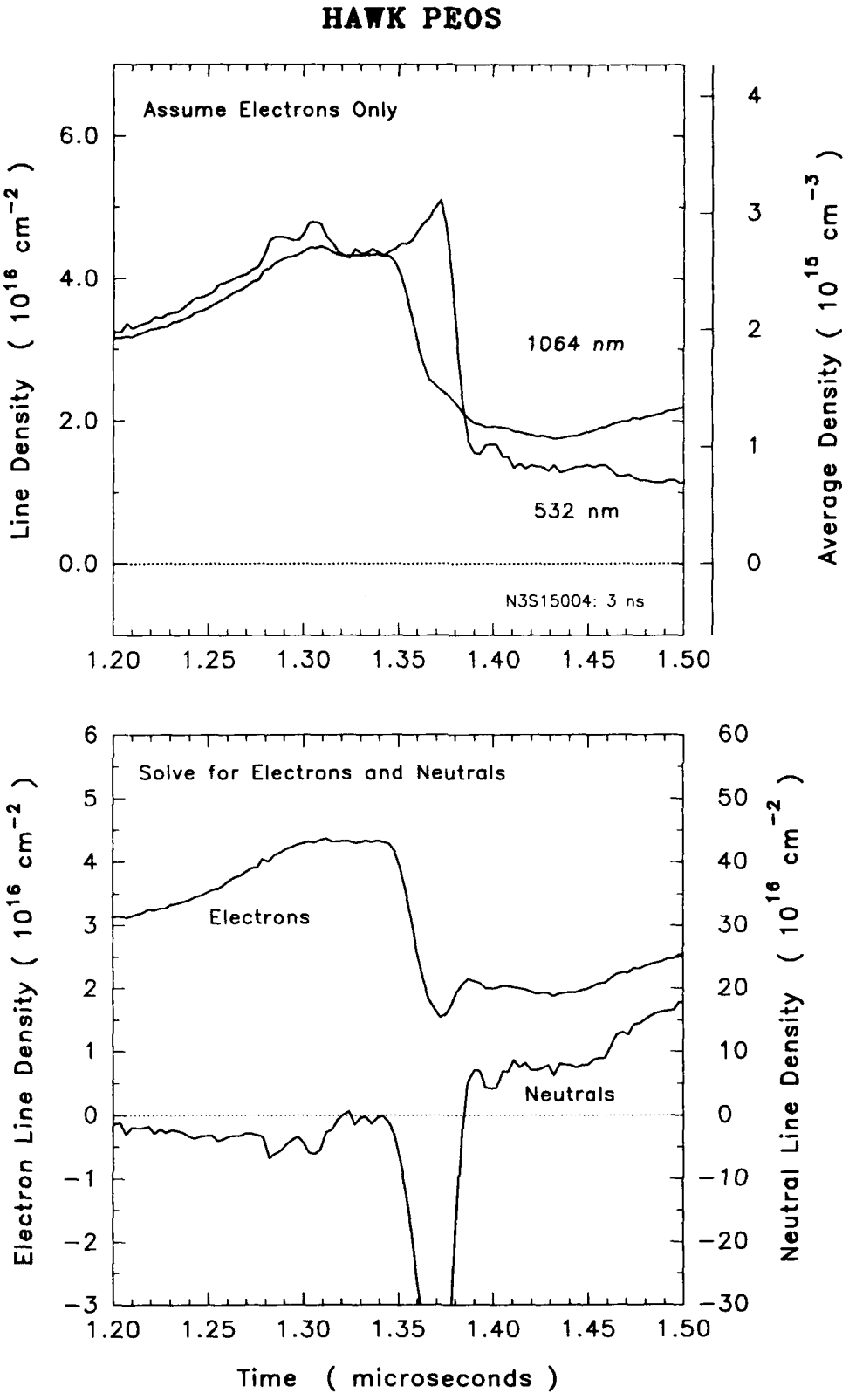

Figure 3-7: Expanded portion of the full HAWK shot plasma measurement.

SECTION 4

OPERATIONS MANUAL

4.1 SAFETY CONSIDERATIONS.

A great virtue of a passive diagnostic such as this one is that it is very difficult to find a way to damage it through improper operation. The only optical elements which might be damaged are the human retinas used in its alignment. This is particularly true in the NRL installation since the optical path being probed is right at eye level.

The lasers supplied to NRL are not particularly powerful, but should be respected. Specular reflections off of optical surfaces and metal objects will be found at times in unexpected places and should be blocked with stops if possible. The 1064 nm beam, being invisible, is of particular concern and the use of IR attenuating safety glasses is highly recommended. The IR safety glasses supplied will pass the orange light produced by the phosphorescent cards used to find the IR beams. Safety goggles for the green probe laser at 532 nm is more problematical because the alignment will be very difficult if all of the wavelengths are blocked. The best course of action is to utilize the fast laser shutters in front of both probe lasers which are opened by supplying a TTL voltage to a BNC input on their front panel of their control boxes. During the alignment the controllers should be provided with 2 ms TTL pulses at a rate of 1 to 2 Hz to produce short laser pulses in the area of the interferometer. The maximum amount of laser energy likely to be absorbed in an eyeball will thus be limited to 200 μJ or less (not harmless, but better than a CW zap). Consult your safety office.

Pulsing the probe lasers during the alignment has other virtues. It is much easier to see the center of the green beam when your eyes are not blinded by a bright focused spot on a card.

Similarly, it is much easier to use the phosphorescent IR beam-finding cards since their "charge" is not depleted as rapidly by the pulsed IR beam.

4.2 SPACE FRAME AND VACUUM HOUSING ASSEMBLY.

Figure 4-1 shows a photograph of the space frame and connecting modules assembled outside of the vacuum housing. Figure 4-2 shows a photograph of the interferometer assembled inside the vacuum housing (which is supported on the roll-around legs supplied to simplify the assembly and installation). In practice, the individual frame components must be assembled inside the vacuum housing in ship-in-a-bottle fashion.

The easiest procedure is to first assemble the four connecting boxes of the vacuum housing with the three connecting tubes. All cover plates are left off at this point with the exception of the bottom cover plates which attach to the roll-around support bars. The horizontal space truss of the frame is assembled separately from the two longer truss sections. Several o-rings are then slipped over the assembled truss to help damp out vibrations in the thin wall stainless tubing. The assembled truss is then placed into the horizontal tube of the vacuum housing through the end holes in the vacuum housing connecting boxes.

The circular rear cover plates on the vacuum housing connecting boxes are then installed. One of these rear cover plates will be the vacuum port with a KF-40 flange welded into its center. The aluminum plate which captures the interferometer as it is lowered is installed in the bottom of the right-hand vacuum housing connecting box. The circular side cover plates for the bottom connecting boxes are then installed. The left side plate, shown in Fig. 4-3, carries the entrance windows to the vacuum housing and the telescopes for viewing the two optical axes.

The vertical space truss assemblies are then lowered into the vacuum housing through the top opening in the connecting boxes (where the spring supports will eventually be placed). These trusses also carry o-rings to damp vibrations.

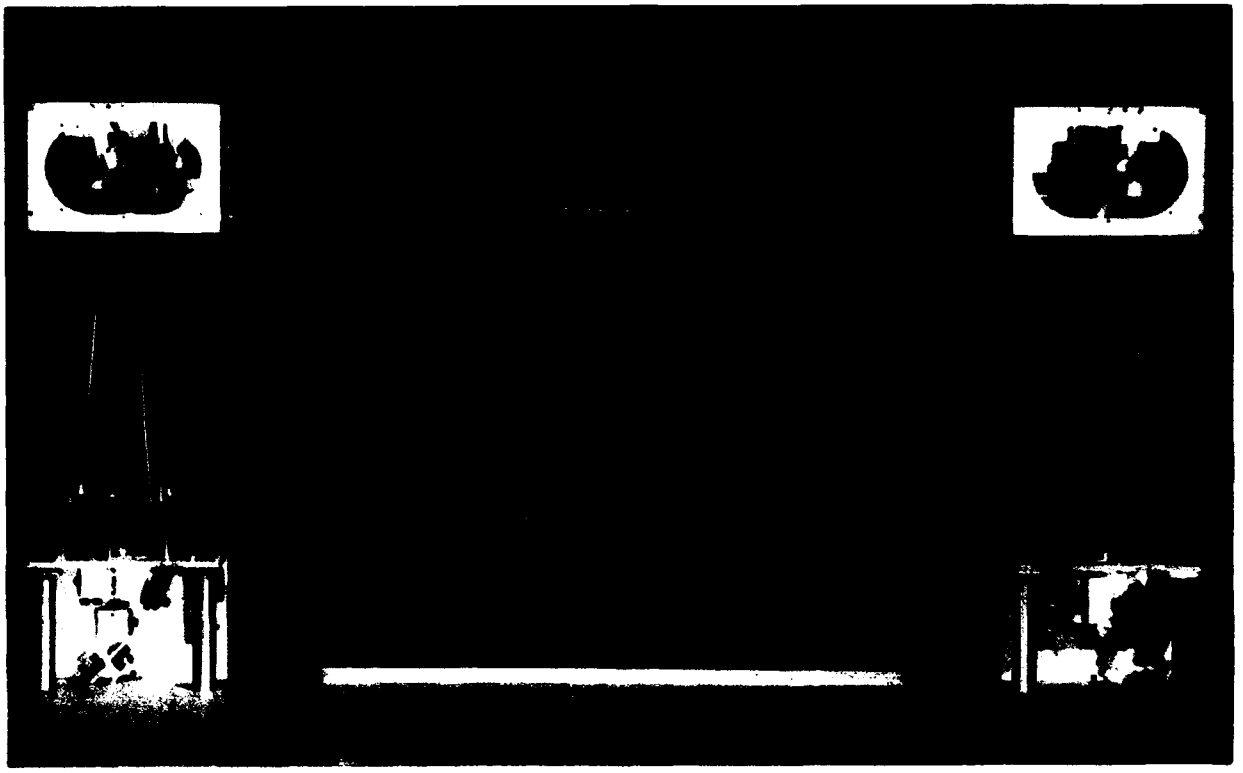

Figure 4-1: Photograph of the interferometer space frame carrying both the 1064 nm and 532 nm interferometers.

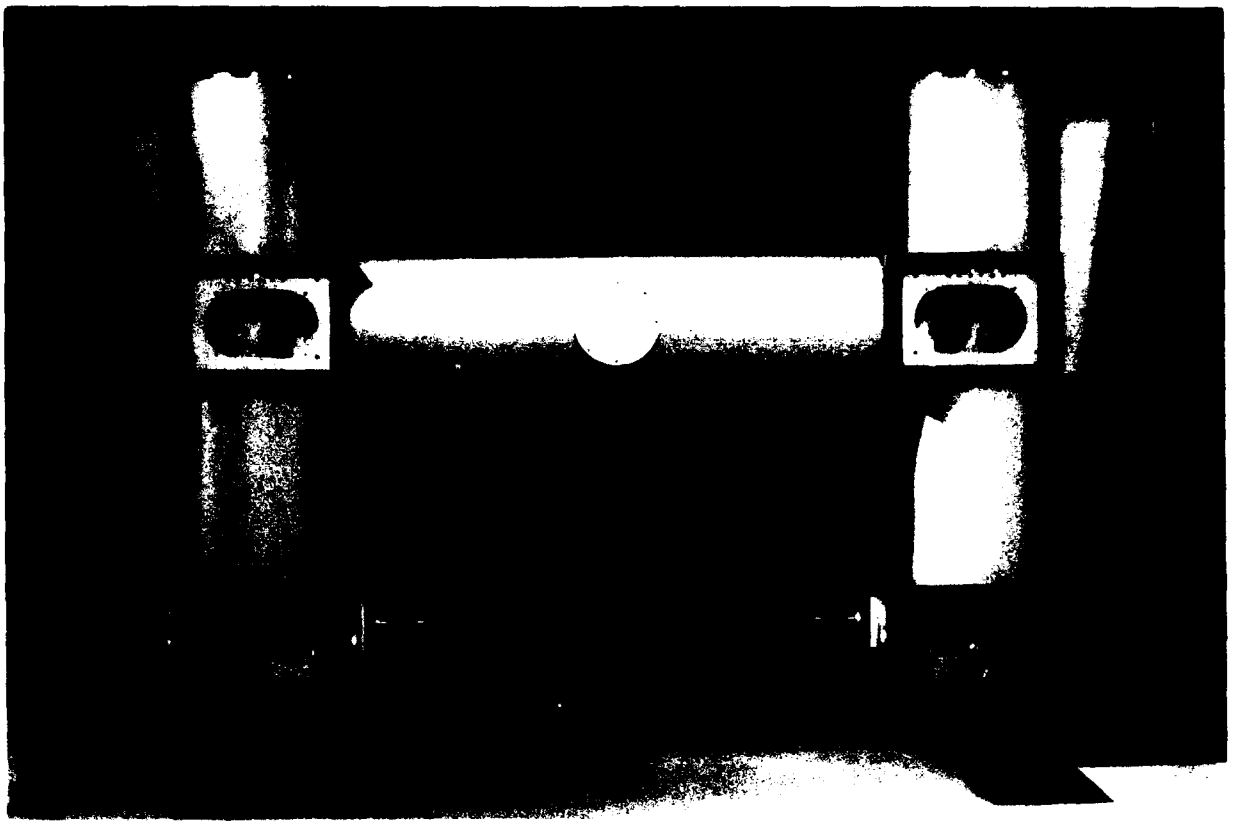

Figure 4-2: Photograph of the vacuum housing containing the interferometers.

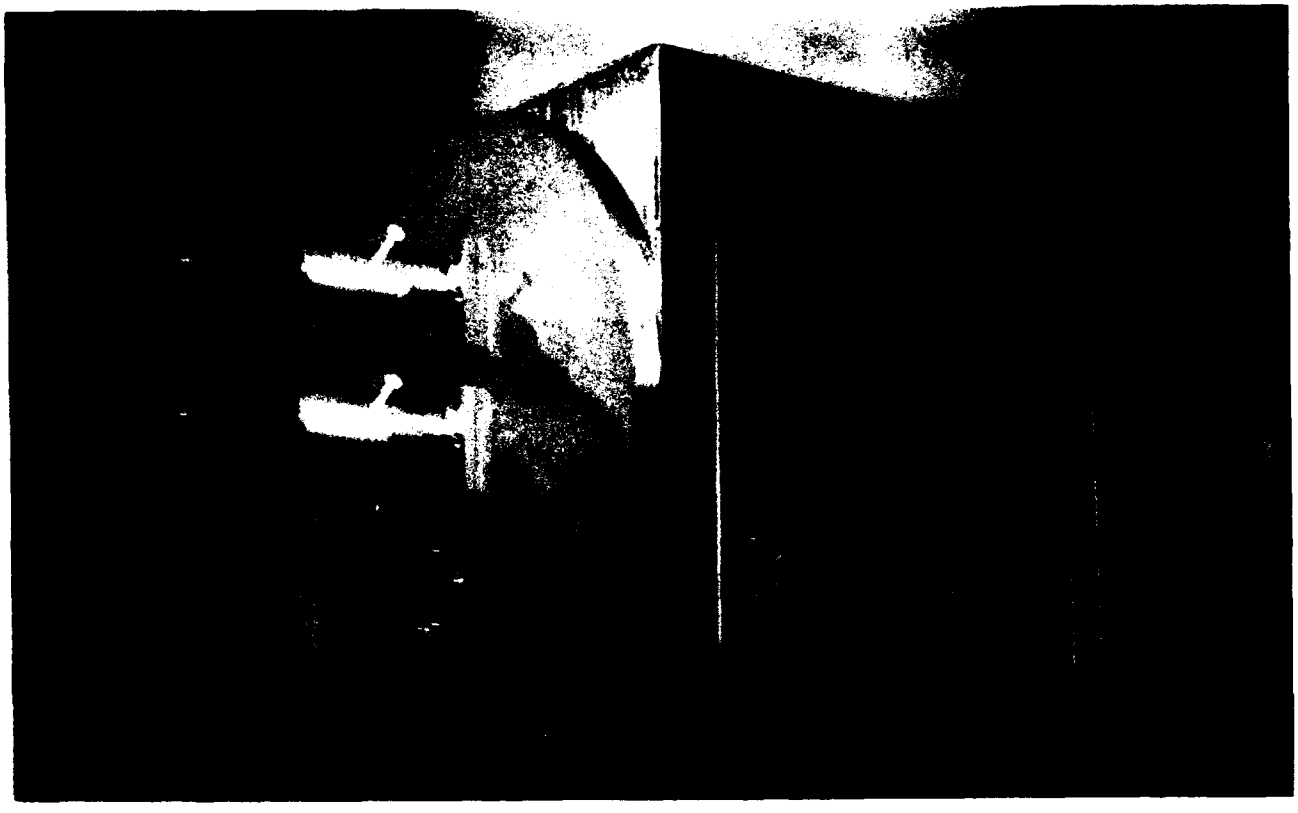

Figure 4-3: Photograph of the entrance side cover on the vacuum housing.

The optical components in the bottom connecting boxes are mounted on aluminum plates. The frames which attach these plates onto the vertical space truss members are slipped in through the front opening of the vacuum housing connecting boxes and attached to the vertical trusses. The plates carrying the optics can be installed later.

The side plates to the top connecting boxes (the blue wing plates which carry the kinematic support points) are then attached, followed by the mounting of the vertical tubes which carry the spring assemblies. These vertical tubes complete the vacuum housing except for the rectangular front cover plates.

At this point the stainless steel connecting boxes for the space frame are installed through the front opening of the vacuum housing connecting boxes and are attached to the vertical and horizontal space trusses.

Once the space frame structure has been assembled inside the vacuum housing the spring suspension system can be dropped into the top of the vertical spring housings and secured with allen head screws from the outside. Figure 2-5 shows the spring assembly. This assembly consists of a ball screw which drives the top plate carrying twenty, soft extension springs. The moving top plate is guided and prevented from rotating by three rods attached to the top cover. The bottom plate where the springs are attached will be itself bolted to the top of the space frame connecting boxes.

The ball screw is driven from the outside by the hand wheel at the top of the assembly. A small o-ring seals the rotating shaft. The ball screw drives the assembly with very little friction so the ratchet and pawl mounted on the outside of the cover plate prevents the ball screw from rotating when the springs are in tension. The springs are kept at a slight extension by the four vertical, pointed rods attached to the bottom plate.

When the top spring plate is driven to its lowest position there is very little force on the bottom spring plate so it can be pulled down to the top of the space frame connecting boxes and attached with allen head bolts. At this point the space frame can be suspended by turning the

hand wheel at the top of the spring housing and stretching the springs until the system floats. About 10 inches of spring extension is required, leading to a natural suspension frequency of about 1 Hz.

When the spring tension is relaxed the space frame settles onto the bottom of the vacuum housing connecting boxes. Four silicone rubber pads cushion it at this point and pins projecting down from the bottoms of each of the space frame connecting boxes fit into guide holes. These pins keep the frame from moving horizontally and the rubber cushions protect it from vertical shock. At the bottom of the space frame, the plate carrying the optics will fit into a guide slot to prevent the space frame from pivoting around its horizontal axis. When the system is moved the suspending assembly should be dropped into this locked position to keep it from banging around inside the vacuum housing.

The plates carrying the passive optical components are now mounted to the bottom of the space frame through the rectangular apertures in the front of the lower vacuum housing connecting boxes. Each of the motorized interferometer mounts in the top quadrants of the interferometer are bolted into place separately through the front apertures of the upper connecting boxes, both inner and outer. These mounts only fit in one way. Their precise positioning is not necessary at this point since they have all of the degrees of freedom they need to align the mirrors and beamsplitters that they carry. Once these motorized mounts are in place, the flexible cable assemblies are connected to provide the power to the motors and the low voltages to the PZT's. These cable assemblies are soldered to the inside of the vacuum feedthroughs attached to the two wing plates covering the side holes of the top vacuum housing connector boxes.

The rectangular front cover plates can be left off until the optics are aligned as described in the following section.

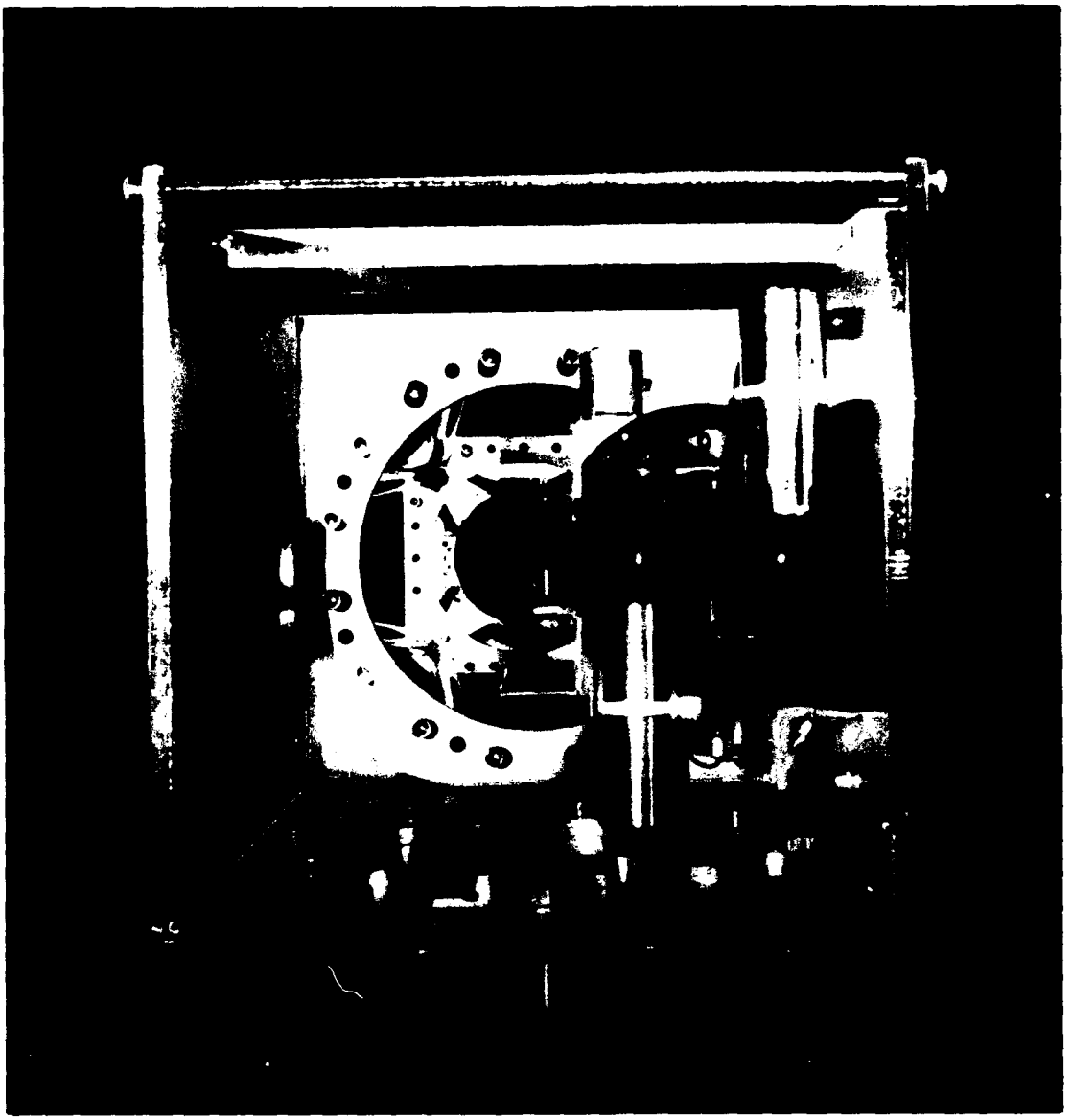

Figure 4-4: Photograph of the guide pins and shock-absorbing pads on the frame.

4.3 OPTICAL ALIGNMENT OF THE INTERFEROMETER.

Figures 4-5, 4-6, 4-7 and 4-8 give a step-by-step procedure for the alignment of the interferometer. This alignment should only need to be performed once for any given experimental setup since the system is designed to be extremely stable. Only occasional adjustments with the remote controls for beam overlap and zero fringes should be necessary on a routine basis. Small adjustments in the positions of the probe beams within the plasma (to go through a small aperture for instance) can be made without affecting the alignment of the interferometer. If the input beams and output beams from the interferometer are parallel, then the position of the beams inside the probed volume is independent of the translational and rotational position of the interferometer. Likewise, if the interferometer is fixed the probe beams can be tipped and tilted through its clear aperture (which, of course, is not very large) without requiring a realignment.

4.4 ELECTRONICS CIRCUITS.

The electronics required for the operation of the SRL plasma diagnostic are comparatively simple and most of the circuits shown have been lifted directly from the cookbooks referenced. Detailed discussions of their operation can be found in those references.

The most important control in the interferometer is the control for the PZT which sets the initial relative phase between the scene beam and the reference beam of the interferometer. The Burleigh PZS-050 translator used provides 50 μm of motion for an input voltage of 150 V, or about 3 volts per wave of the IR probe. Since only one wave or so of motion is required the DC voltage was provided by a 9 V battery and a 10-turn potentiometer. The PZT appears as a capacitive load so it draws no current. The interferometer was stable to about 0.001 waves of drift per second so a biofeedback loop was used to hold the proper phase (someone to turn

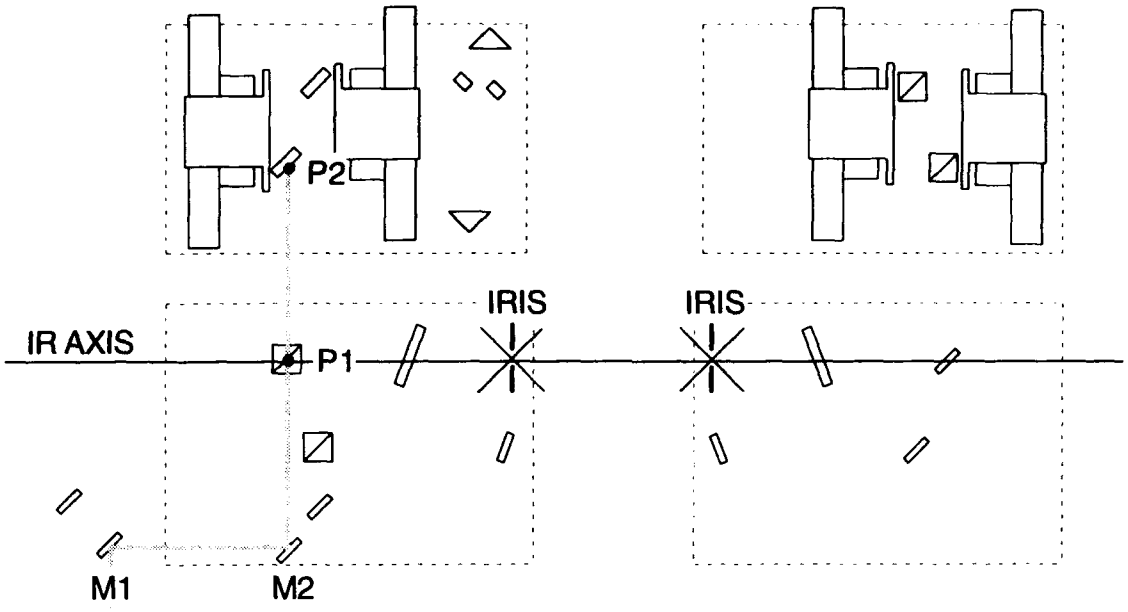

Step 1: Align IR beam through point P1 (defined by intersection of iris axis and beamsplitter prism) and P2 (defined by center of mirror) using mirrors M1 and M2.

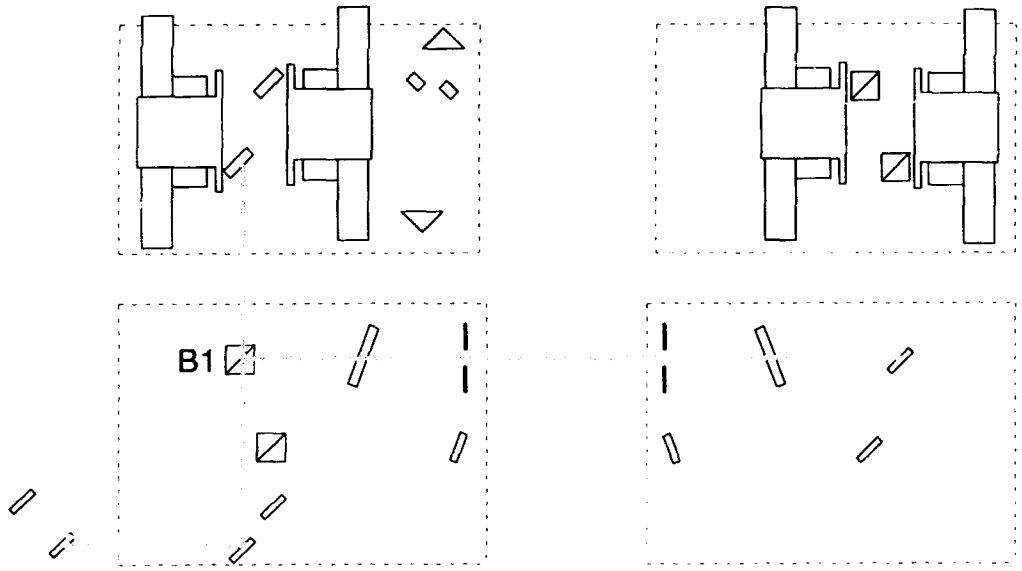

Step 2: Align IR scene beam through iris centers by tilting and rotating beamsplitter prism B1. Since this beam defines point P1 it may be necessary to iterate Step 1 and Step 2.

align1

Figure 4-5: Alignment of the IR probe onto the scene beam axis.

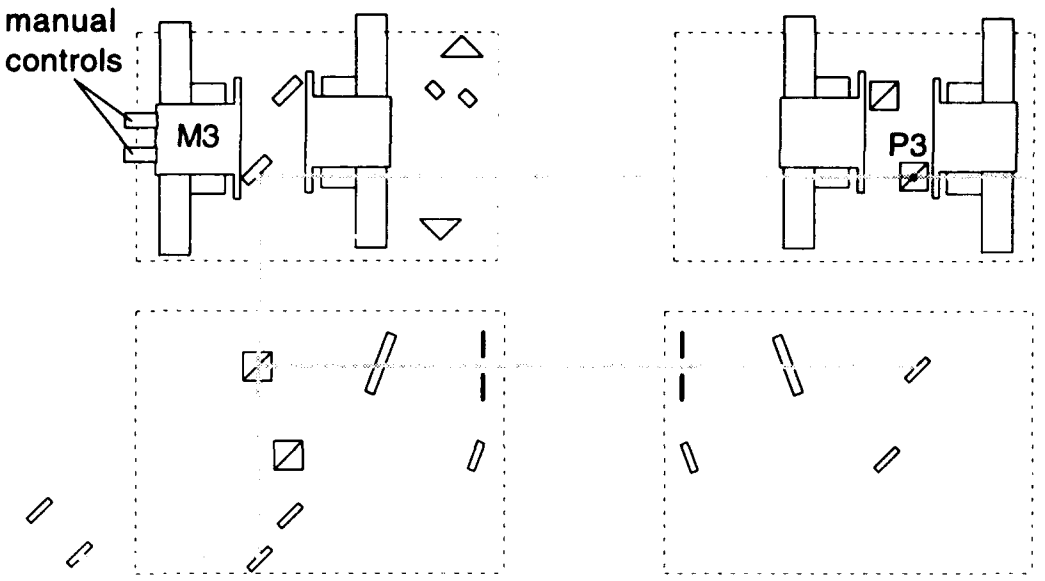

Step 3: Align IR reference beam through point P3 (defined by the center of the beam combiner prism) using manual controls on mirror mount M3. Make sure motorized micrometers are roughly centered in their travel at this time.

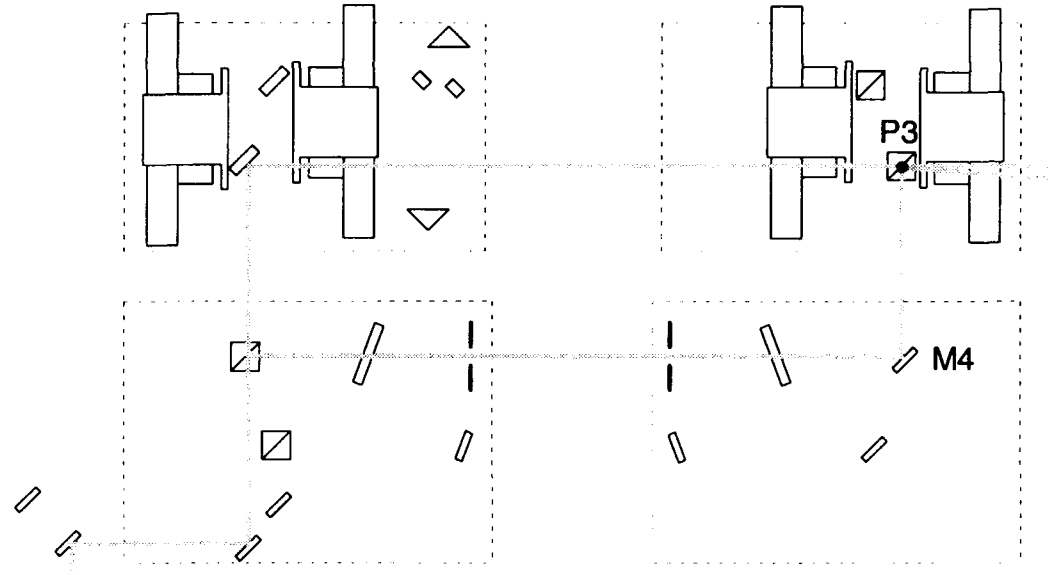

Step 4: Align IR scene beam through point P3 using mirror mount M4. This is most easily checked by looking at the beam reflected from the beam combiner prism at a point very near the prism. Blocking the reference beam will help to distinguish the two.

align2

Figure 4-6: Alignment of the IR reference beam to the output beamsplitter.

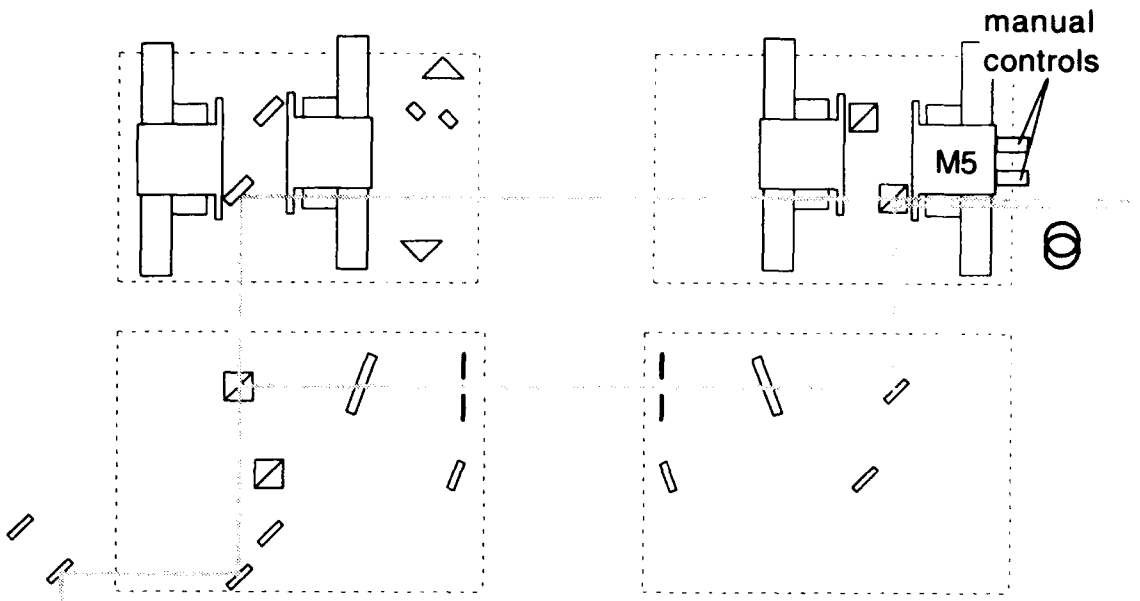

Step 5: Align the axes of the IR scene and reference beams using the manual controls of M5 (checking again to make sure micrometer moters are roughly centered in their travel). From this point on the beams can be aligned remotely.

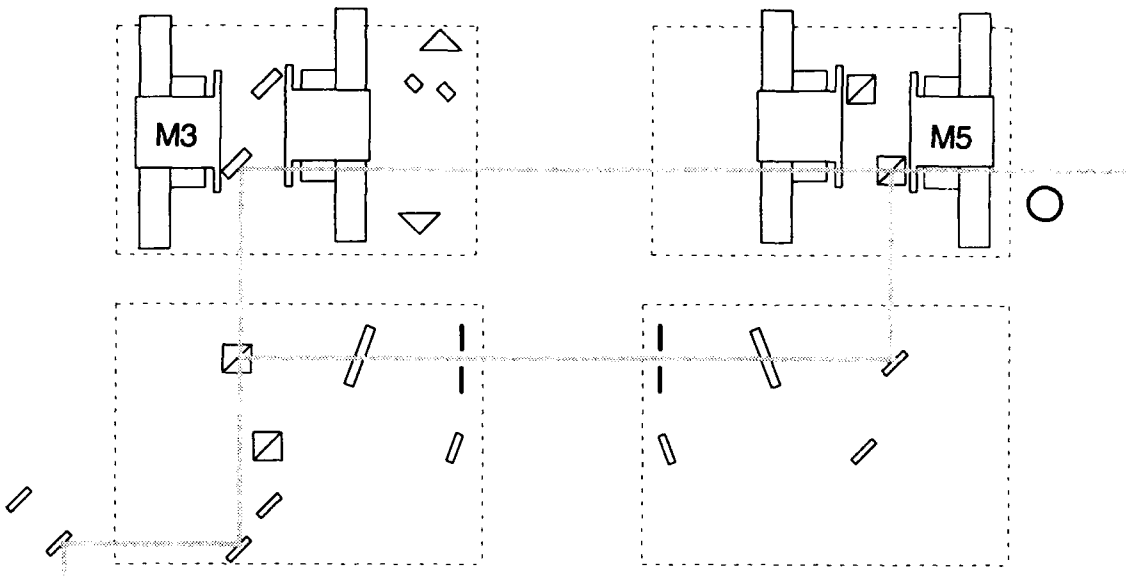

Step 6: Iterate between adjusting mirror mounts M3 and M5 using the motorized micrometers until the beam overlap and the zero fringe conditions are met.

align3

Figure 4-7: IR probe overlap and fringe control (manual or remote).

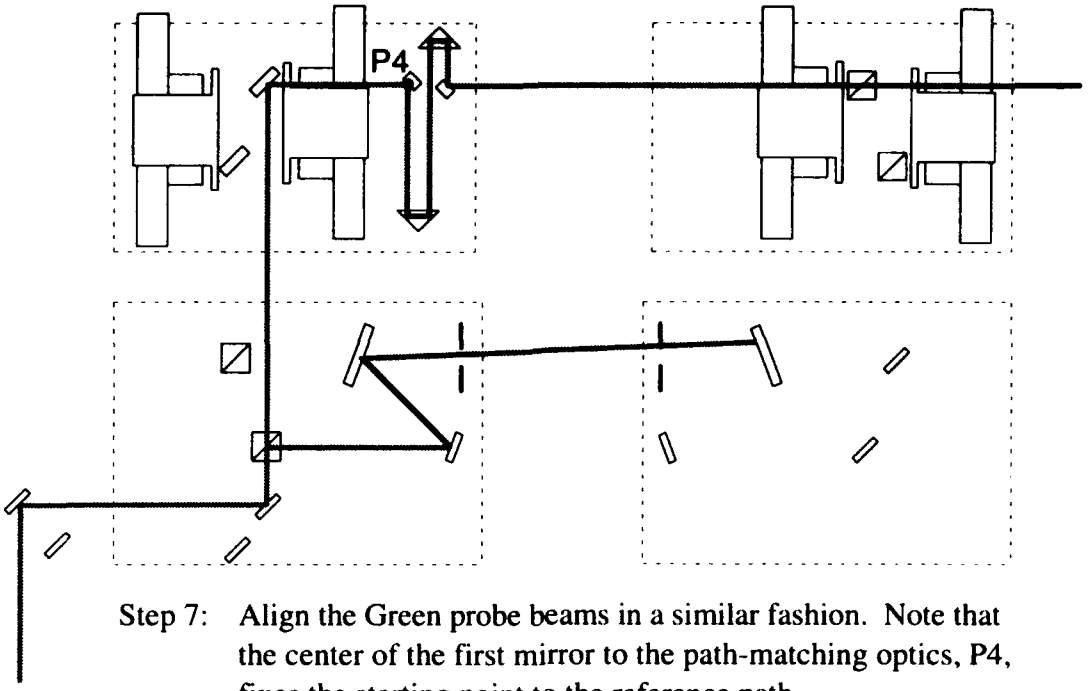

Step 7: Align the Green probe beams in a similar fashion. Note that the center of the first mirror to the path-matching optics, P4, fixes the starting point to the reference path.

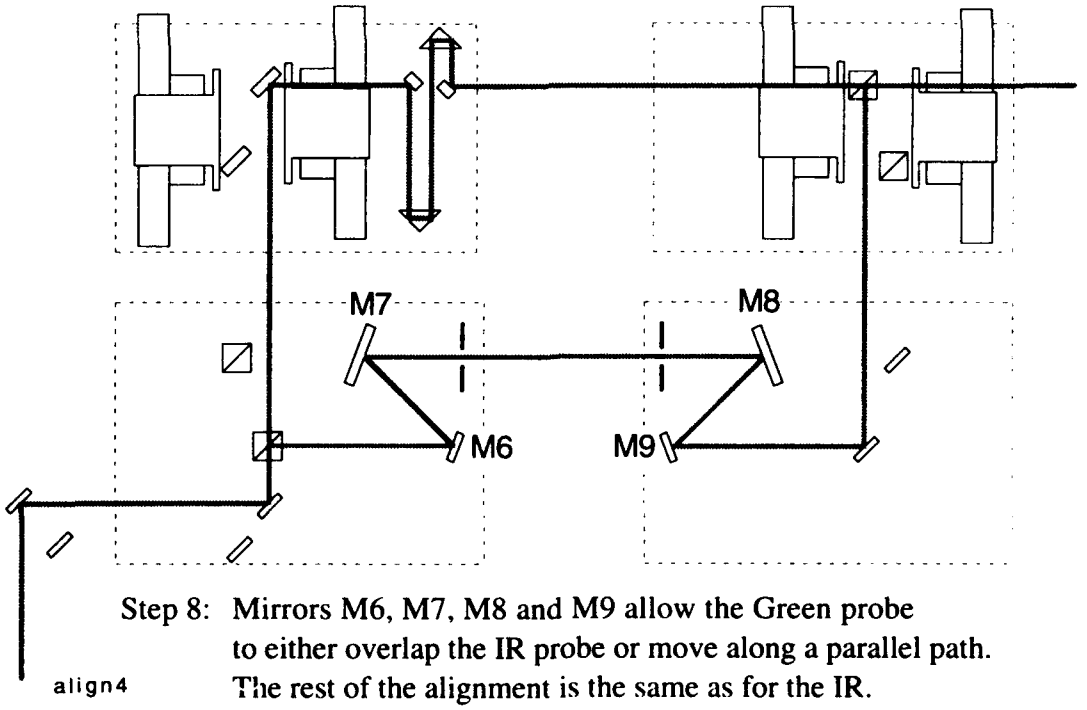

Step 8: Mirrors M6, M7, M8 and M9 allow the Green probe to either overlap the IR probe or move along a parallel path. The rest of the alignment is the same as for the IR.

align4

Figure 4-8: Differences between the 532 nm probe and 1064 nm probe alignment.

a knob when necessary). The feedback information was coupled out of the screen room to the potentiometers with two Q-tip sticks.

In the future, however, a feedback loop may prove useful so a simple circuit was built and tested at NRL. This circuit, shown in Fig. 4-9, worked fine, reducing the drift rate by about a factor of 20 (its loop gain). It wasn't used in the experiments because it did not provide for the feedback information to be coupled out optically. Wires coming from the screen room would have picked up electrical noise and compromised the data. The LeCroy digital oscilloscope was triggered, by the way, with a fast fiber optic trigger link from the HAWK timing system. This link was provided by SRL.

A simple modification to the feedback loop, shown in Fig. 4-10, would provide an optical link back to the interferometer PZT's. This circuit uses an HP HFBR-2208 photodiode as the fiber optic receiver because it couples directly to the fiber but does not draw battery current when there is no light coming in from the fiber. The receiver could thus be attached right at the interferometer and would not have to be switched off when it was not being used. Note that in this design the loop gain is controlled by the load resistors in the receiver. The fiber optic link components could not be delivered before the termination of the contract. If the system is to be built the additional components will have to be purchased and assembled by NRL.

The plasma diagnostic signal voltage is proportional to the electron density (and at its most sensitive point) when the photodiode bridge voltage is zero. For the most sensitive two-color measurements both bridge voltages must be near zero when the plasma is generated. The window comparator circuit shown in Fig. 4-11 indicates when the voltage on each bridge is either negative (red LED is on) or positive (yellow LED is on). When BOTH bridge voltages are within a small window around zero a green LED is illuminated. This is the circuit used to close the biofeedback loop in most of the NRL experiments. The operator in the screen room controlling the data acquisition would adjust the two knobs (inside the screen room) attached by

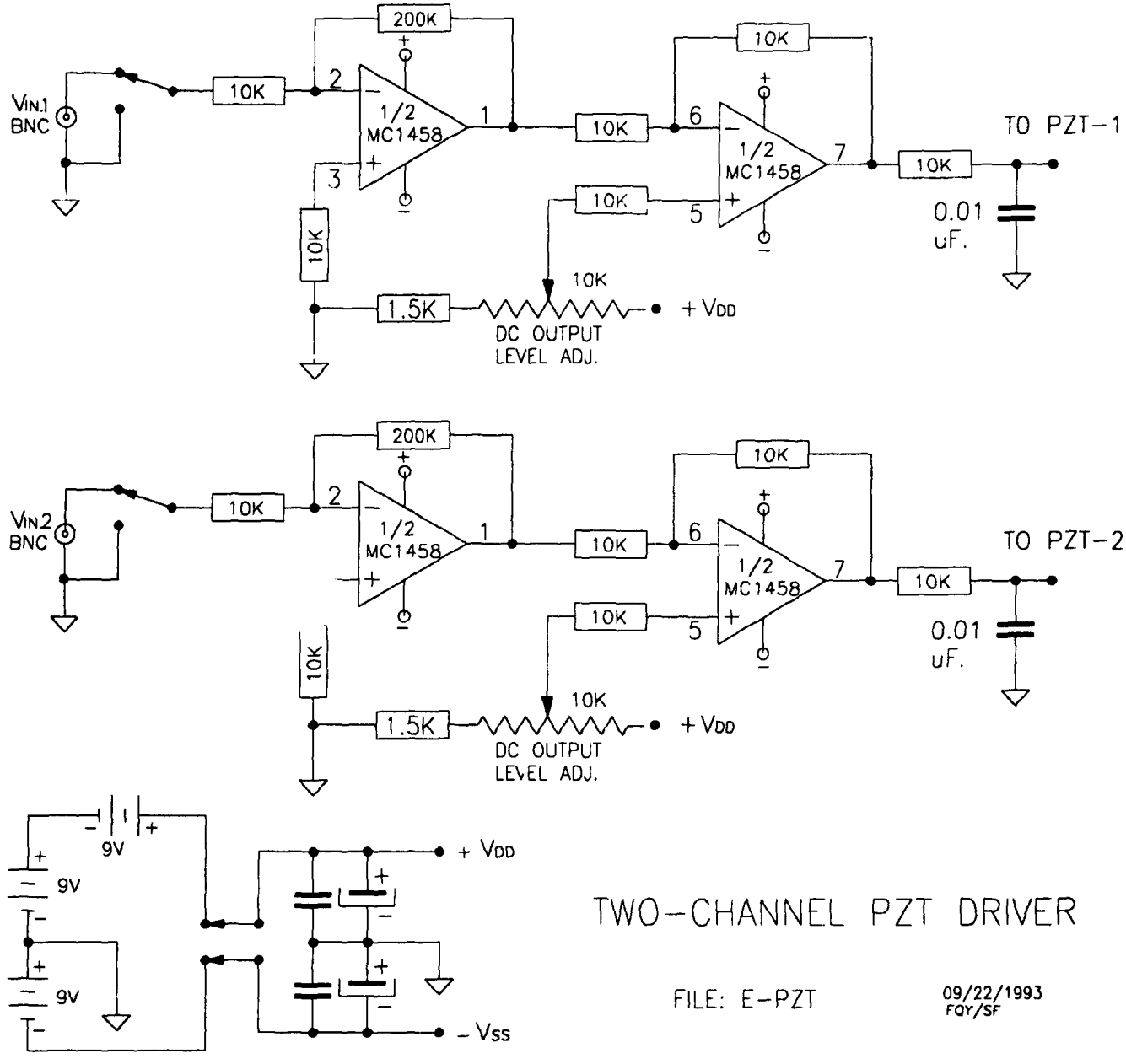

Figure 4-9: PZT feedback loop for the SRL plasma diagnostic as tested at NRL.

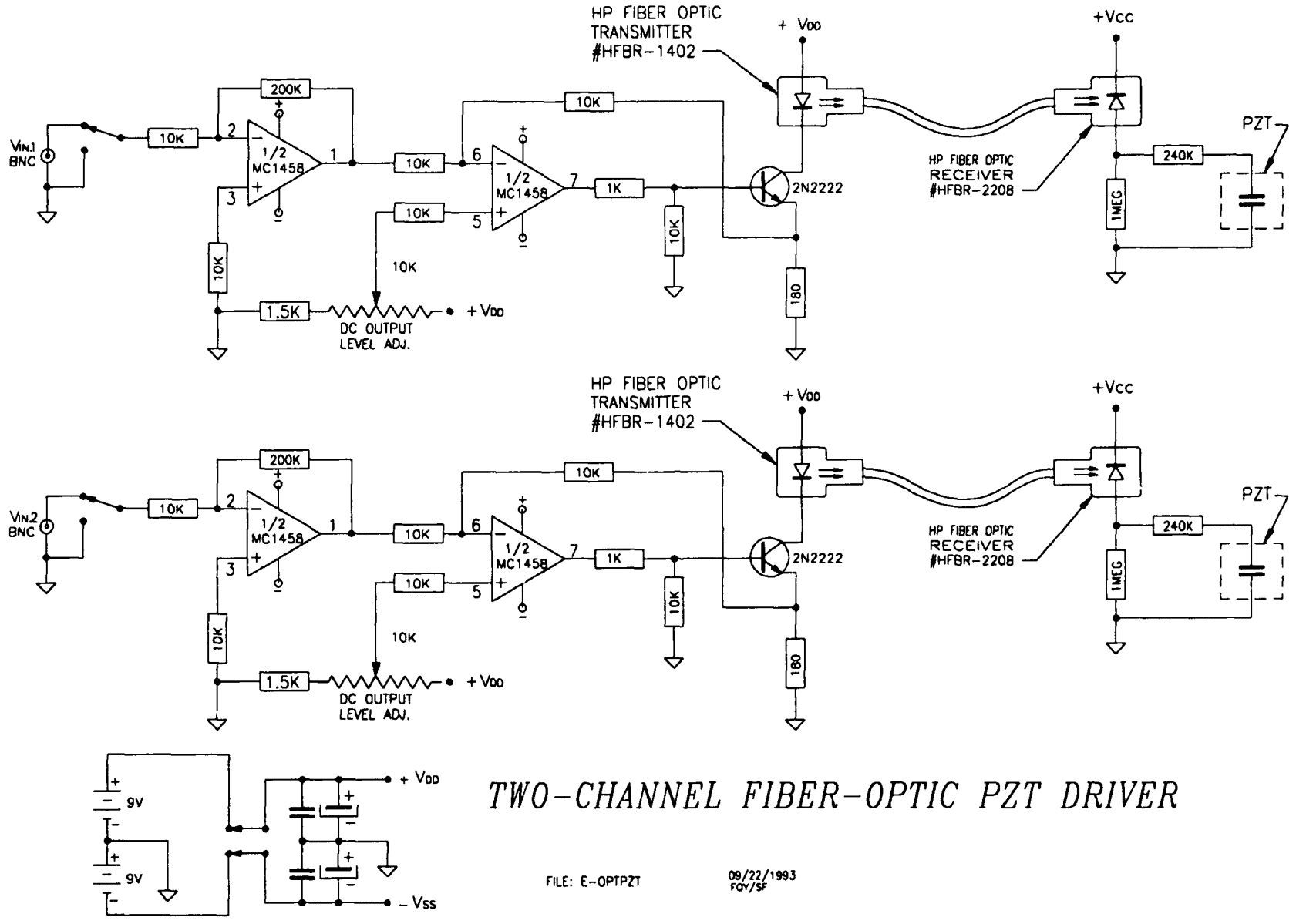

Figure 4-10: PZT feedback loop for the SRL plasma diagnostic with a proposed fiber optic link out of the screen room.

Q-tip sticks to the PZT battery box (outside the screen room) to keep the green LED illuminated. The HAWK PEOS could then be fired whenever its operators wished.

A suggested modification to this basic comparator circuit is shown in Fig. 4-12. There are two basic changes from the design used in the original experiments. One variation provides for a variable window voltage center as well as a variable window voltage span. These comparator circuits are described in the cookbooks by Jung and Mims referenced on the circuit drawing. This modification would simplify holding a desired offset voltage for experiments with large electron density swings. The second modification provides for a fiber optic transmitter to indicate to an outside trigger circuit (to be described) when both bridges were within their voltage tolerance. By setting the window spans to very small values a series of closely spaced spikes would be optically transmitted as the two bridge circuits swept through their (combined) optimal settings. The rising edge of any one of these trigger pulses could serve as a trigger for the HAWK firing sequence.

If HAWK were to be fired by the modified comparator circuit an additional trigger circuit would be required prior to the existing HAWK timing circuits. This is because the HAWK trigger system will fire repeatedly as trigger pulses are applied to it. A circuit is needed to select just one incoming trigger pulse and ignore the rest. Figure 4-13 shows a circuit which has long been used at SRL to provide a single trigger pulse from a series of possible triggers at a time selected by the push of a button. The circuit is a simple set/reset, monostable flip-flop built of NAND gates. The circuit is ARMED (but not fired) by grounding one of its inputs with a manual reset button (debounced). This action causes the output of the flip-flop to transition from a high state to a low state, turning on a green "armed" LED in the process as a visual indicator. The flip-flop output will switch back to its high state when its other input is grounded. The other input of the flip-flop is attached to the output of a dual-input NAND gate. This NAND gate will only trigger the flip-flop high state output when BOTH a trigger pulse from the screen room AND a 250 ms pulse from a manual FIRE command appear simultaneously on its inputs. The triggers from the screen room are coming continuously at a high rate (if the window span is small enough). The

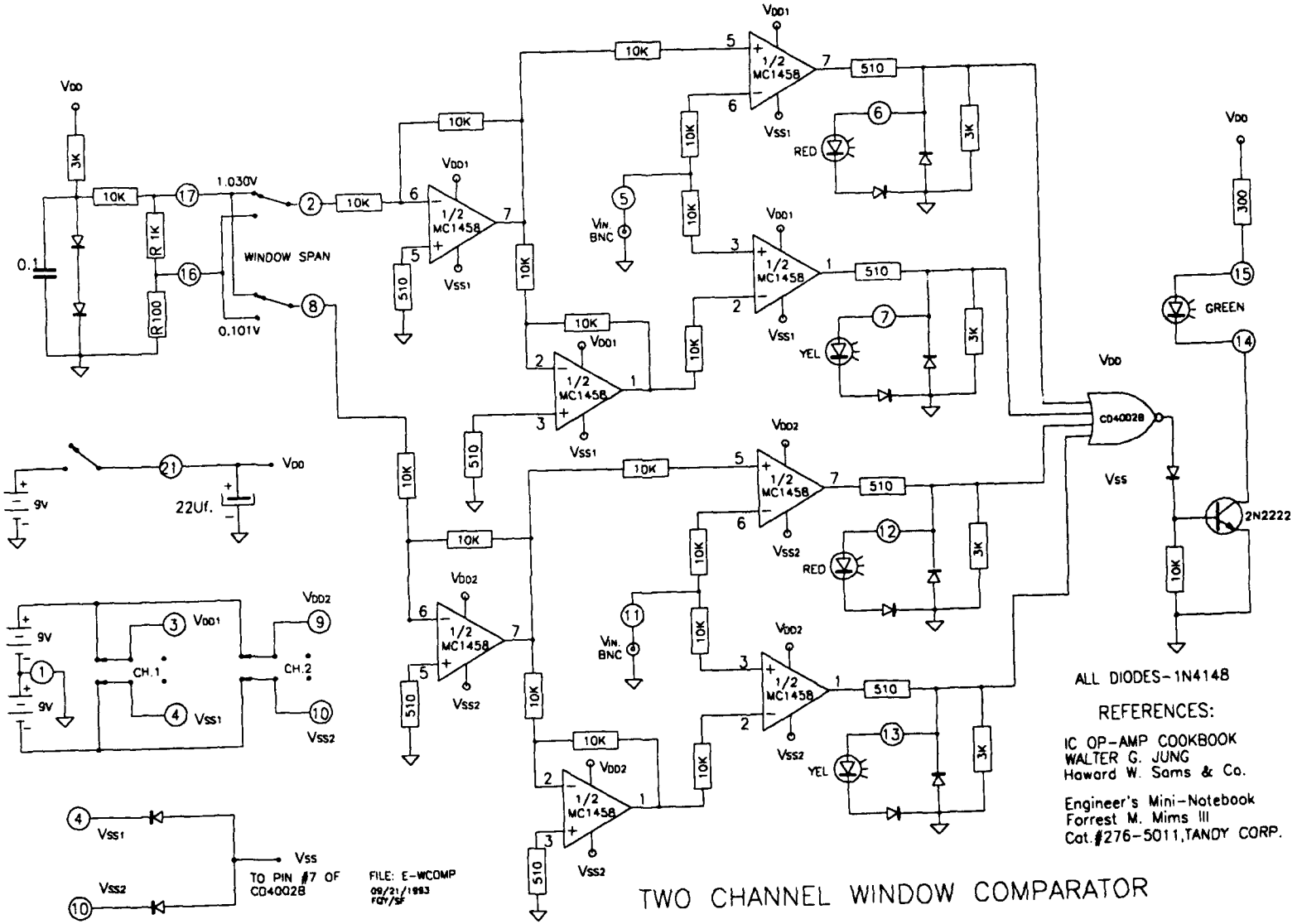

Figure 4-11: Circuit used in the NRL experiments to keep both bridge circuits at their optimal balance.

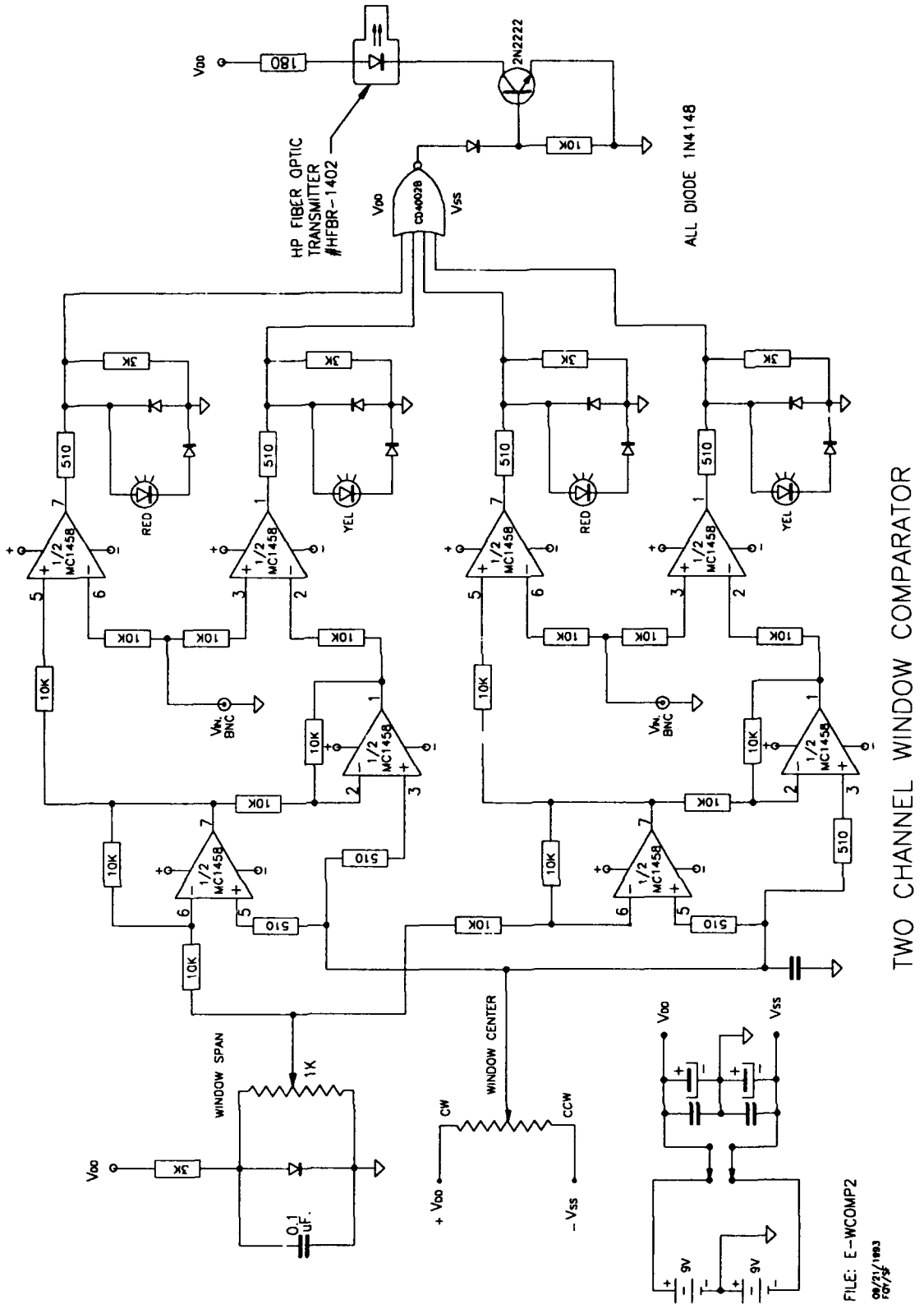

Figure 4-12: Suggested modifications to the window comparator circuit.

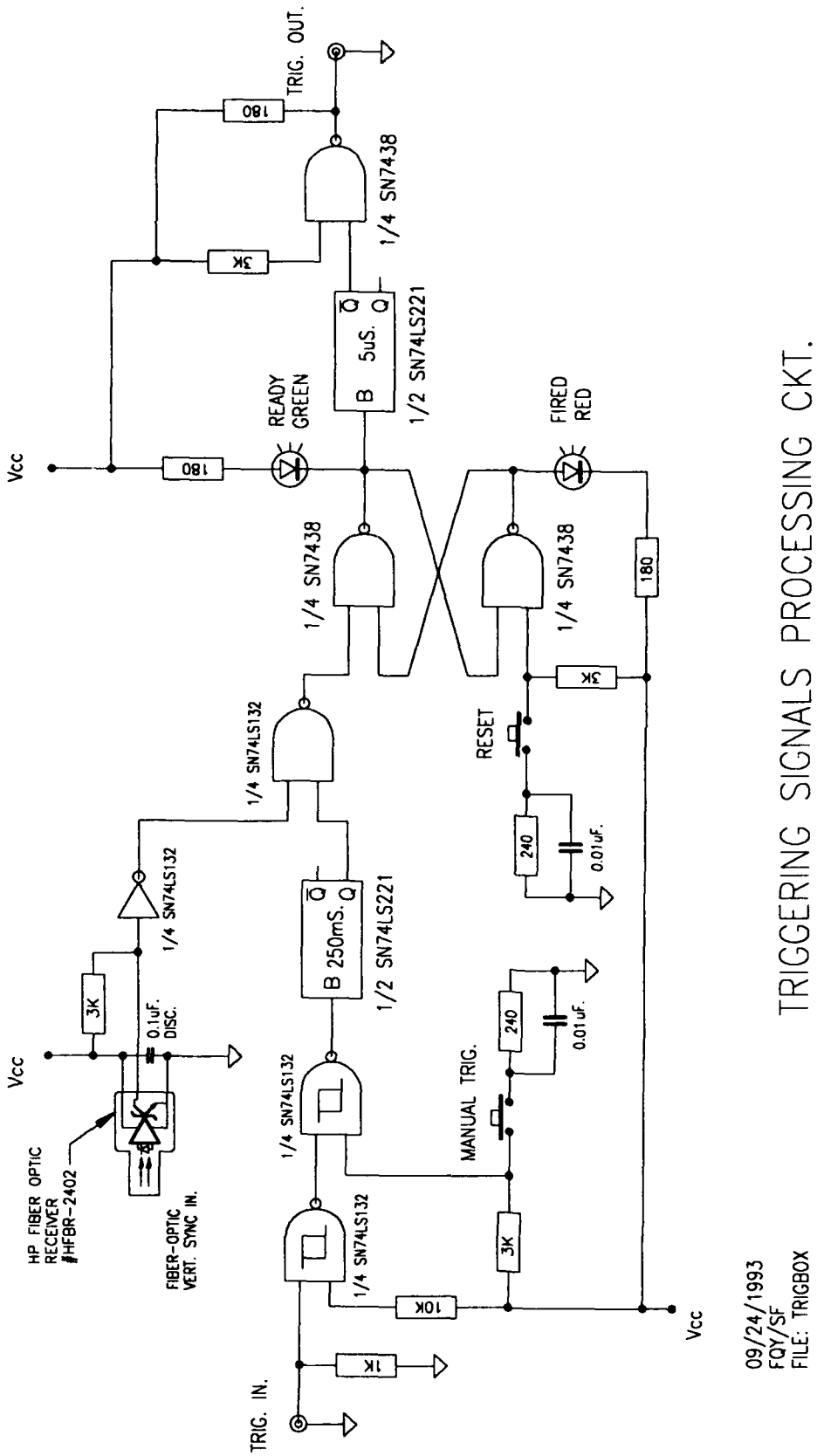

Figure 4-13: Suggested trigger circuit to optically connect HAWK to a modified window comparator circuit.

HAWK operator selects the time when he wants to send the FIRE command. The 1/4 second duration for the FIRE command provides the operator the opportunity to abort the shot if for some reason the triggers are not coming from the screen room at the rate expected. The operator can press the FIRE button again if the system didn't trigger the first time. The actual 5 μs TTL trigger out of this circuit is produced by a fixed length monostable multivibrator chip which is triggered by the rising edge of the output of the set/reset flip-flop. The high state of the flip-flop output causes a red "fired" LED to light. Note that this circuit will only provide one output pulse no matter how many times the FIRE button is pressed. To trigger the HAWK system a second time the RESET button must be pushed (turning on the "armed" LED) followed by the FIRE button.

4.5 VIBRATION ISOLATION TABLES.

The vibration isolation table supplied to NRL to support the SRL plasma diagnostic on HAWK, shown in Fig.2-8, has been designed to be as general in its purpose as possible. The table can be set up on four tubular steel legs, as shown in Fig. 4-14, to allow the diagnostic to be used separately from HAWK. This might be desirable if the system were to be used in studies of flashboards with its own vacuum chamber mounted to the vacuum housing. Plates with tapped bolt holes are also welded to several faces of the table frame to allow it to be attached easily to structures other than HAWK.

The table attaches to HAWK through the use of a 2×4 inch tubular steel bar attached to the bolt circle of the circular flange at the end of the Marx bank chamber. The table is rigidly attached to this bar in the rear while thin tubular steel posts under the front legs take up its weight in compression. The thin legs do not provide any lateral stability. Four such identical legs have been provided to hold the table at the appropriate height for HAWK if the system needs to be moved farther from the wall in later experiments (i.e. axial measurements using

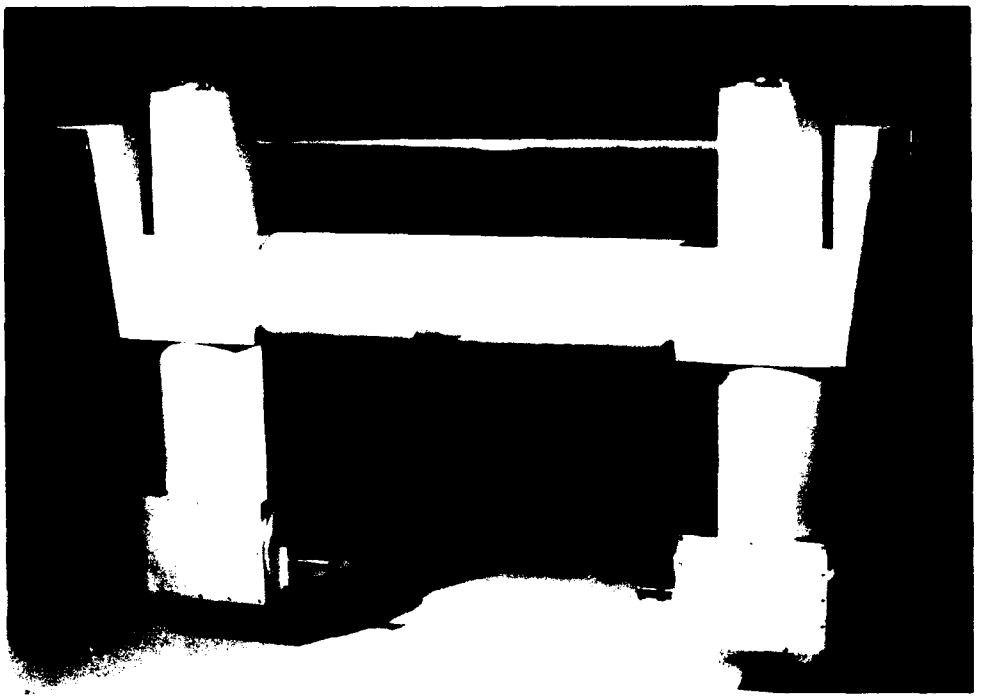

Figure 4-14: Photograph of the stand-alone support frame for the system.

retroreflectors attached to HAWK). In this case additional structural members would be required between the table and the wall to provide lateral stability.

4.6 ANALYSIS PROGRAMS.

The analysis of the data from the SRL plasma diagnostic is also relatively straightforward. A listing of the C program used in the reduction of the data at SRL is provided in the Appendix.

REFERENCES

1. D. Reilly, "Visible wavelength interferometer for high speed electron density measurements," Final Techn. Rep. (sponsored by the Defense Advanced Research Projects Agency under contract N60921-82-C-0141, monitored by the Naval Surface Weapons Center, White Oak, Silver Spring, Md. (Avco Everett Research Laboratory, Everett Mass., June 1984).

2. B.V. Weber and D.D. Hinshelwood, "He-Ne interferometer for density measurements in plasma opening switch experiments", Rev. Sci. Instrum. **63**, 5199-5201 (1992).

3. R.A. Bosch, H. Ching, R.M. Gilgenbach, P.L.G. Ventzek, P.R. Menge, J.J. Choi and T.A. Spencer, "Deflection of carbon dioxide laser and helium-neon laser beams in a long-pulse relativistic electron beam diode", Rev. Sci. Instrum, **62**, 1776-1782 (1991).

4. S. F. Fulghum, "Laser Interferometric Characterization of Plasma Densities," Phase I SBIR Final Report, Defense Nuclear Agency Contract DNA001-90-C-0113.

5. S.F. Fulghum, "Multi-Beam Laser Interferometer for Plasma Density Measurements in a Plasma Erosion Opening Switch (PEOS)," Phase II SBIR Proposal to Defense Nuclear Agency, May 30, 1991.

6. S.F. Fulghum and M.M. Tilleman, "Interferometric calorimeter for the measurement of water vapor absorption," J. Opt. Soc. Am. B, **8**, 2402-2413 (1991).

7. G.R. Fowles, *Introduction to Modern Optics*, Holt, Rinehart and Winston, New York, 1968.

8. M. Born and E. Wolf, *Principles of Optics*, Pergammon Press, Oxford, 6th ed. (with corrections) 1980.

9. The author would like to thank Dr. Peter Rostler, who has recently joined SRL, for these calculations.

10. W.L. Wiese and G.A. Martin, "Atomic Spectroscopy," Chapter 5 in *Physics Vade Mecum*, H.L. Anderson, Ed., Amer. Inst. of Phys., 1981.

APPENDIX

Analysis of Two-Color Data

```
/* REDUC0.C

27 Sep 93  Stephen F. Fulghum
Science Research Laboratory, 15 Ward St., Somerville, MA 02143
OFFICE: (617) 547-1122   FAX: (617) 547-4104

Calculates the electron and neutral densities measured
by the SRL Plasma Diagnostic Interferometer.

Outputs data in an ASCII file for plotting with columns:
(1) time in microseconds
(2) 1064 data (IR) analyzed individually and interpreted either as
    electron density (NeL) or neutral density (rhoL) depending
    on an option input to the analysis program.
(3) 532 nm data (GR) analyzed individually and interpreted either as
    electron density (NeL) or neutral density (rhoL) depending
    on an option input to the analysis program.
(4) Electron density as determined from the two colors.
(5) Neutral density as determined from the two colors.
Columns separated by TAB, lines ended with LF.

Inputs:

  (A) Lecroy binary data files trace1.xxx and trace2.xxx of the
      voltages on the 1064 nm (IR) and 532 nm (GR) photodiode bridges
      (where xxx is the sequential shot number assigned by the scope)
      measured by the Lecroy 7200 Oscilloscope and converted to ASCII
      as XXXXXXXX.IR0 and XXXXXXXX.GR0 using Lecroy's WAVETRAN program
      (where XXXXXXXX is the shot name assigned by the user).
      The IR0 and GR0 descriptors are assumed by this analysis program.

  (B) Maximum and minimum voltages measured on both photodiode bridges
      during a sweep through several waves on the interferometers
      accomplished by applying voltages sweeps to their PZT's.
      (As measured directly at the bridge load resistor.)

  (C) The gain applied to the above voltages by the Stanford Research
      Systems amplifiers (must be either 5X, 25X or 125X).

  (D) The Horizontal Offset, ie. the time of the first Lecroy data sample
      relative to the scope trigger as determined by WAVETRAN using the
      -d switch to write out the waveform descriptor.

  (E) The sampling period (typically 1 ns) as determined by WAVETRAN.

with the Options:

  (F) Choice of an analysis window of N samples inside of which the
      data samples will be averaged.  This reduces both noise and plot
      file size at the expense of signal bandwidth.
```

```
   (G) The choice of the baseline subtraction method, AVERAGE or SLOPE,
       where AVERAGE is a simple average over the baseline before the
       scope trigger and SLOPE fits a + bt so that a linear slope can
       be subtracted during the data period after the trigger.

   (H) The choice of a specific period in the pretrigger data over which
       to fit the baseline so that signals from flashboards triggered
       before the scope can be avoided.

   (I) The choice of individually analyzing the 1064 nm and 532 nm data
       as either electron density or neutral density for output.

Procedure:

   (1) Reads both raw input data files  XXXXXXXX.IR0 and .GR0.
   (2) Calculates the baseline phase for the IR and GR probes.

   Loops through data file, calculating results and writing to output.

   (3) Averages samples in widow.
   (4) Calculates the phase shift from the voltage
       assuming that the photodiode signal stays linear so that
       the phase can be calculated simply by assuming a sinusoidal
       signal variation with phase.
   (5) Inverts IR phase and GR phase to electron line densities and
       neutral line densities, then inverts the 2x2 matrix to recover
       the electron density and neutral density from both measurements.
   (6) Calculates the averaged window's time relative to the trigger
       in units of microseconds by adding the time offset with the time
       assigned being the center of the window.
   (7) Outputs a single data file as: time(usec), IR NeL, GR NeL
       (or IR rhoL, GR rhoL), NeL, rhoL /LF.

*/
/* ************************************************************************ */
#include <stdio.h>
#include <process.h>
#include <math.h>
#include <string.h>
#include <conio.h>
#include <ctype.h>

void main()
{
  FILE *fpIR,*fpGR,*fpout;
  char basename[40],IRfile[40],GRfile[40],outfile[40];
  int cbase,cshow;
  int i,window;
  float tdelta,tbasestart,tbasestop,toutstart,toutstop;
  float value,sum,VIRavg,VGRavg,t,toffset;
  float S,Sx,Sy,Sxx,Sxy,VIRa,VIRb,VGRa,VGRb,VIRstart,VGRstart;
```

```
  float VIRhigh,VIRlow,VGRhigh,VGRlow,VIRzero,VGRzero,VIRamp,VGRamp;
  float count,phaseIR0,phaseGR0;
  float phaseIR,phaseGR;
  float lambdaIR=(float)1.064e-4;  /* wavelength of IR probe, cm */
  float lambdaGR=(float)0.532e-4;  /* wavelength of green probe, cm */
  float re=(float)2.82e-13;        /* classical radius of the electron, cm */

  /* beta= delta n in cm^3 units assuming N2 which is 3e-4 atm-1 */
  /* this may be changed later if more is known about the plasma */

  float beta=(float)1.0e-23;

  float NeLIR,NeLGR;
  float rhoLIR,rhoLGR;
  float NeL,rhoL;
  float IRcalibfactor,GRcalibfactor;

/* ------------------------------------------------------------------- */
/* set up file names */

  printf("Reduc0: 27 Sep 93, S.F.Fulghum, Science Research Laboratory\n\n");
  printf("Input base file name, .IR0, .GR0 assumed\n");

  scanf(" %s",basename);

  strcpy(IRfile,basename);
  strcpy(GRfile,basename);
  strcpy(outfile,basename);
  strcat(IRfile,".IR0");
  strcat(GRfile,".GR0");
  strcat(outfile,".ALL");
  printf("Reading %s and %s\n",IRfile,GRfile);
  printf("Writing %s\n\n",outfile);

  fpIR=fopen(IRfile,"r");
  if(fpIR==NULL) {
    printf("Can't open file %s\n",IRfile);
    exit(1);
  }
  fpGR=fopen(GRfile,"r");
  if(fpGR==NULL) {
    printf("Can't open file %s\n",GRfile);
    exit(1);
  }
  fpout=fopen(outfile,"w");
  if(fpout==NULL) {
    printf("Can't open file %s\n",outfile);
    exit(1);
  }

  fprintf(fpout,
```

```
    "Reduc0: 26 Sep 93, S.F.Fulghum, Science Research Laboratory\n");

/* ---------------------------------------------------------------------- */
/* get horizontal time offset (trigger time) */

  printf("Enter the Horizontal Offset time value in microseconds\n");
  scanf(" %f",&toffset);
  printf("Adding %g microseconds to sample times\n\n",toffset);

  printf("Enter the digitization period in nanoseconds\n");
  scanf(" %f",&tdelta);
  printf("Digitizes every %5.1f nanoseconds\n\n",tdelta);

  printf("Enter the number of periods to be averaged\n");
  scanf(" %d",&window);
  printf("Averaging %d samples\n\n",window);

  printf("Enter start time in microseconds for baseline averaging\n");
  scanf(" %f",&tbasestart);
  printf("Baseline starts at: %5.2f microseconds\n\n",tbasestart);

  printf("Enter stop time in microseconds for baseline averaging\n");
  scanf(" %f",&tbasestop);
  printf("Baseline stops at: %5.2f microseconds\n\n",tbasestop);

  printf("Enter start time in microseconds for output data\n");
  scanf(" %f",&toutstart);
  printf("Start time for output is: %5.2f microseconds\n\n",toutstart);

  printf("Enter stop time in microseconds for output data\n");
  scanf(" %f",&toutstop);
  printf("Stop time for output is: %5.2f microseconds\n\n",toutstop);

  cbase='_';
  do {
    printf("To subtract AVERAGE baseline enter ''a''\n");
    printf("To subtract LINEAR baseline enter ''l''\n\n");
    cbase=tolower(getch());
  } while (!( (cbase=='a')||(cbase=='l') ));
  if (cbase=='a') {
    printf("AVERAGE baseline to be subtracted\n");
    fprintf(fpout,"average baseline from %5.2f to %5.2f microseconds\n"
     ,tbasestart,tbasestop);
  } else {
    printf("LINEAR baseline to be subtracted\n\n");
    fprintf(fpout,"linear baseline from %5.2f to %5.2f microseconds\n"
     ,tbasestart,tbasestop);
  }

  cshow='_';
  do {
```

```
    printf("To analyze each trace as ELECTRONS enter ''e''\n");
    printf("To analyze each trace as NEUTRALS enter ''n''\n\n");
    cshow=tolower(getch());
  } while (!( (cshow=='e')||(cshow=='n') ));
  if (cshow=='e') {
    printf("Output table shows individual traces as ELECTRONS\n\n");
    fprintf(fpout,"t(1e-6s), NeL 1064, NeL 532, NeL, rhoL (1e16cm-2)\n");
  } else {
    printf("Output table shows individual traces as NEUTRALS\n\n");
    fprintf(fpout,"t(1e-6s), rhoL 1064, rhoL 532, NeL, rhoL (1e16cm-2)\n");
  }

/* ------------------------------------------------------------------- */
/* get peak positive and negative voltage swings for both IR and GR */

  printf("Enter voltage swings for IR and GReen probes\n");
  printf("enter IR high voltage: ");
  scanf(" %f",&VIRhigh);

  printf("enter IR low  voltage: ");
  scanf(" %f",&VIRlow);

  printf("enter GR high voltage: ");
  scanf(" %f",&VGRhigh);

  printf("enter GR low  voltage: ");
  scanf(" %f",&VGRlow);

  printf("\nIR swing is from %g to %g volts\n",VIRhigh,VIRlow);
  printf("GR swing is from %g to %g volts\n\n",VGRhigh,VGRlow);
  fprintf(fpout,"IRhi:%6.3f, IRlo:%6.3f, GRhi:%6.3f, GRlo:%6.3f\n",
   VIRhigh,VIRlow,VGRhigh,VGRlow);

  VIRzero=(VIRhigh+VIRlow)/(float)2;
  VGRzero=(VGRhigh+VGRlow)/(float)2;
  VIRamp=(VIRhigh-VIRlow)/(float)2;
  VGRamp=(VGRhigh-VGRlow)/(float)2;
  printf("IR voltage zero: %7.4f,  IR voltage amplitude: %7.4f\n",
    VIRzero,VIRamp);
  printf("GR voltage zero: %7.4f,  GR voltage amplitude: %7.4f\n\n",
    VGRzero,VGRamp);

/* ------------------------------------------------------------------- */
/* Factor in calibration corrections */

  printf("enter additional calibration factor (gain?) for IR: ");
  scanf(" %f",&IRcalibfactor);

  printf("enter additional calibration factor (gain?) for GR: ");
  scanf(" %f",&GRcalibfactor);
```

```
  VIRamp*=IRcalibfactor;
  VGRamp*=GRcalibfactor;

  printf("\nIR calibration factor: %6.4f\n",IRcalibfactor);
  printf("\nGR calibration factor: %6.4f\n\n",GRcalibfactor);
  fprintf(fpout,"IRfactor:%7.3f, GRfactor:%7.3f\n",
   IRcalibfactor,GRcalibfactor);

/* ------------------------------------------------------------------ */
/* Calculate the average slope to the IR and GR baselines
   from tbasestart to tbasestop (to allow for pretriggered plasmas).
   Set the initial phase to the fit value at t=tbasestop.
*/

   t=toffset;   /* time of first sample */
   S=(float)0; Sx=(float)0; Sy=(float)0; Sxx=(float)0; Sxy=(float)0;
   while(t<tbasestop) {
     fscanf(fpIR," %f",&value);
     if(t>tbasestart) {
       S+=(float)1;
       Sx+=(float)t;
       Sy+=value;
       Sxx+=t*t;
       Sxy+=t*value;
     }
     t+=(float)0.001*tdelta;
   }
   rewind(fpIR);
   VIRa=(Sxx*Sy-Sx*Sxy)/(S*Sxx-Sx*Sx);
   VIRb=(S*Sxy-Sx*Sy)/(S*Sxx-Sx*Sx);
   VIRavg=Sy/S;
   printf("IR baseline avg V: %8.5f, linear: %8.5f +(%8.5f*t)\n",
    VIRavg,VIRa,VIRb);
   if (cbase=='a') VIRstart=VIRavg;
     else VIRstart=VIRa +VIRb*tbasestop;
   phaseIR0=(float)asin( (VIRstart-VIRzero)/VIRamp );
   printf("Initial IR baseline voltage: %7.4f\n",VIRstart);
   printf("Initial IR phase: %8.5f\n\n",phaseIR0);

   t=toffset;   /* time of first sample */
   S=(float)0; Sx=(float)0; Sy=(float)0; Sxx=(float)0; Sxy=(float)0;
   while(t<tbasestop) {
     fscanf(fpGR," %f",&value);
     if(t>tbasestart) {
       S+=(float)1;
       Sx+=(float)t;
       Sy+=value;
       Sxx+=t*t;
       Sxy+=t*value;
     }
     t+=(float)0.001*tdelta;
```

```
   }
   rewind(fpGR);
   VGRa=(Sxx*Sy-Sx*Sxy)/(S*Sxx-Sx*Sx);
   VGRb=(S*Sxy-Sx*Sy)/(S*Sxx-Sx*Sx);
   VGRavg=Sy/S;
   printf("GR baseline avg V: %8.5f, linear: %8.5f + (%8.5f*t)\n",
    VGRavg,VGRa,VGRb);
   if (cbase=='a') VGRstart=VGRavg;
     else VGRstart=VGRa +VGRb*tbasestop;
   phaseGR0=(float)asin( (VGRstart-VGRzero)/VGRamp );
   printf("Initial GR baseline voltage: %7.4f\n",VGRstart);
   printf("Initial GR phase: %8.5f\n\n",phaseGR0);

/* ================================================================== */
/* Data Averaging Loop */

  printf("Averaging windows in data files\n");
  t=toffset +window*tdelta/(float)2000;   /* usec of first avg sample */
  do {

/* ================================================================== */
/* Average a window of samples from each input file.
   Make a baseline correction using the a abd b parameters
   calculated for the baseline.
*/

   sum=(float)0;
   for(i=0;i<window;i++) {
     fscanf(fpIR," %f",&value);
     sum+=value;
   }
   VIRavg=(sum/(float)window);
   if (cbase=='l') VIRavg-=VIRb*(t+tbasestop);

   sum=(float)0;
   for(i=0;i<window;i++) {
     fscanf(fpGR," %f",&value);
     sum+=value;
   }
   VGRavg=sum/(float)window;
   if (cbase=='l') VGRavg-=VGRb*(t+tbasestop);

/* ------------------------------------------------------------------ */
/* Convert volts to phase using sinusoid fit */
/* NOTE phase negation on green to account for analyzer rotation */

   phaseIR=(float)asin( (VIRavg-VIRzero)/VIRamp );
   phaseGR=(float)asin( (VGRavg-VGRzero)/VGRamp );

/* ------------------------------------------------------------------ */
/* Analyze traces separately assuming only electrons */
```

```
/* NOTE!  Green result is inverted to account for analyzer rotation */

   NeLIR=(phaseIR - phaseIR0)/(re * lambdaIR);
   NeLGR=-(phaseGR - phaseGR0)/(re * lambdaGR);

/* ------------------------------------------------------------------ */
/* Analyze traces separately assuming only neutrals */
/* NOTE!  Green result is inverted to account for analyzer rotation */

   rhoLIR=-(phaseIR - phaseIR0)*lambdaIR/(6.2832*beta);
   rhoLGR=(phaseGR - phaseGR0)*lambdaGR/(6.2832*beta);

/* ------------------------------------------------------------------ */
/* Invert to give NeL and rhoL */
/* NOTE!  Green result is inverted to account for analyzer rotation */

   NeL=(phaseIR - phaseIR0)*lambdaIR + (phaseGR-phaseGR0)*lambdaGR;
   NeL/=(-re)*(lambdaGR*lambdaGR-lambdaIR*lambdaIR);

   rhoL=(phaseIR - phaseIR0)*lambdaGR + (phaseGR-phaseGR0)*lambdaIR;
   rhoL/=(-6.2832*beta)*(lambdaGR/lambdaIR-lambdaIR/lambdaGR);

/*------------------------------------------------------------------ */
/* scale results for plot file.  time already in microseconds */

  NeLIR/=(float)1.0e16;
  NeLGR/=(float)1.0e16;
  rhoLIR/=(float)1.0e16;
  rhoLGR/=(float)1.0e16;
  NeL/=(float)1.0e16;
  rhoL/=(float)1.0e16;

/*------------------------------------------------------------------ */
/* Print result to output file */

   if( !feof(fpIR) && !feof(fpGR) && t>=toutstart ) {
     if(cshow=='e') fprintf(fpout,"%7.3f\t%11.3e\t%11.3e\t%11.3e\t%11.3e\n",
       t,NeLIR,NeLGR,NeL,rhoL);
     else fprintf(fpout,"%7.3f\t%11.3e\t%11.3e\t%11.3e\t%11.3e\n",
    t,rhoLIR,rhoLGR,NeL,rhoL);
   }
/* ------------------------------------------------------------------ */
/* increment time (in microseconds) for next averaged data point */
/* Assumes scope timebase set for 1 ns per sample */

   t+=(float)window*tdelta/(float)1000;

/* ================================================================== */
/* End: Data Averaging Loop */

   } while( !feof(fpIR) && !feof(fpGR) && t<=toutstop );
```

```
/* ========================================================================== */
/* Clean up and go home */

  fclose(fpIR);
  fclose(fpGR);
  fclose(fpout);
  printf("finis\n");

}
/* ************************************************************************** */
/* END of REDUC0.C */
```

DISTRIBUTION LIST

DNA-TR-93-147

DEPARTMENT OF DEFENSE

ASSISTANT TO THE SECRETARY OF DEFENSE
ATTN: EXECUTIVE ASSISTANT

BALLISTIC MISSILE DEFENSE ORGANIZATION
ATTN: DTI D DUSTON

DEFENSE INTELLIGENCE AGENCY
ATTN: DIW-4

DEFENSE NUCLEAR AGENCY
ATTN: RAST K WARE
ATTN: SPSD P SENSENY
ATTN: SPWE
ATTN: SPWE B TUCKER
ATTN: SPWE E TREMBA
ATTN: SPWE K PETERSEN
ATTN: TDTR
2 CY ATTN: TITL

DEFENSE TECHNICAL INFORMATION CENTER
2 CY ATTN: DTIC/OC

FIELD COMMAND DEFENSE NUCLEAR AGENCY
ATTN: FCNV M O'BRIEN

FIELD COMMAND DEFENSE NUCLEAR AGENCY
ATTN: FCTI G S LU
ATTN: FCTO
ATTN: FCTT-T E RINEHART
ATTN: FCTT-T W SUMMA
ATTN: FCTT DR BALADI

DEPARTMENT OF THE ARMY

ARMY RESEARCH LABORATORIES
ATTN: ANSRL-WT-NH G HUTTLIN
ATTN: F AGEE
ATTN: SLCHD-NW-HPM S GRAYBILL
ATTN: SLCHD-NW-RS
ATTN: SLCHD-NW-RS M BUSHELL

ELECTRONICS TECH & DEVICES LAB
ATTN: PULSE POWER CTR
ATTN: SLCET-D C THORNTON

U S ARMY BALLISTIC RESEARCH LAB
ATTN: SLCBR-SS-T

U S ARMY COLD REGION RES & ENG LAB
ATTN: CECRL-MAILROOM

U S ARMY ENGR WATERWAYS EXPER STATION
ATTN: C WELCH CEWES-SE-R
ATTN: J INGRAM WESSER
ATTN: RESEARCH LIBRARY

U S ARMY NUCLEAR & CHEMICAL AGENCY
ATTN: MONA-NU DR D BASH

DEPARTMENT OF THE NAVY

DAVID TAYLOR RESEARCH CENTER
ATTN: CODE 1770

NAVAL POSTGRADUATE SCHOOL
ATTN: CODE 61SW F SCHWIRZKE

NAVAL RESEARCH LABORATORY
ATTN: CODE 4770 G COOPERSTEIN
ATTN: CODE 4770 R COMMISSO
ATTN: CODE 6700 S OSSAKOW
ATTN: CODE 6750 R MEGER

NAVAL SURFACE WARFARE CENTER
ATTN: CODE H23 V KENYON
ATTN: CODE R14 R BARSH
ATTN: CODE R15 R B TUSSING

NAVAL SURFACE WARFARE CENTER
ATTN: CODE B-20

DEPARTMENT OF THE AIR FORCE

AFIS/INT
ATTN: INT

AIR FORCE ARMAMENT LABORATORY
ATTN: A BRINSON
ATTN: D WATTS

AIR FORCE OFFICE OF SCIENTIFIC RSCH
ATTN: DR R BARKER

AIR UNIVERSITY LIBRARY
ATTN: AUL-LSE

PHILLIPS LABORATORY
ATTN: LIBRARY

DEPARTMENT OF ENERGY

LAWRENCE LIVERMORE NATIONAL LABORATORY
ATTN: ALLEN KUHL

LOS ALAMOS NATIONAL LABORATORY
ATTN: C OSLEN
ATTN: J OGLE
ATTN: CHARLES FENSTERMACHER
ATTN: R REINOVSKY
ATTN: J BROWNELL

SANDIA NATIONAL LABORATORIES
ATTN: A CHABAI DIV 9312
ATTN: DIV 2566 J HARRIS
ATTN: DIV 9341 J LEE
ATTN: M BUTTRAM DIV 1248
ATTN: ORG 9300 J E POWELL
ATTN: ORG 9340 W BEEZHOLD
ATTN: TECH LIB 3141

OTHER GOVERNMENT

CENTRAL INTELLIGENCE AGENCY
ATTN: OSWR/NED
ATTN: OSWR J PINA

NASA
ATTN: J LEE

NATIONAL INSTITUTE OF STANDARDS & TECHNOLOGY
ATTN: R HEBNER

DEPARTMENT OF DEFENSE CONTRACTORS

AEROSPACE CORP
ATTN: LIBRARY ACQUISITION

APPLIED PHYSICAL ELECTRONICS RESEARCH CENTER
ATTN: DR W NUNNALLY

APPLIED RESEARCH ASSOCIATES, INC
ATTN: J KEEFER
ATTN: N ETHRIDGE

APPLIED RESEARCH ASSOCIATES, INC
ATTN: C J HIGGINS
ATTN: F E SEUSY

BERKELEY RSCH ASSOCIATES, INC
ATTN: N PEREIRA

FLUID PHYSICS IND
ATTN: R TRACI

GEO CENTERS, INC
ATTN: B NELSON

IIT RESEARCH INSTITUTE
ATTN: DOCUMENTS LIBRARY

JAYCOR
ATTN: J STUHMILLER

JAYCOR
ATTN: CYRUS P KNOWLES

KAMAN SCIENCES CORP
ATTN: D BRYCE
ATTN: J CHUNG

KAMAN SCIENCES CORP
ATTN: D MOFFETT
ATTN: DASIAC

KAMAN SCIENCES CORPORATION
ATTN: DASIAC

LOGICON R & D ASSOCIATES
ATTN: C K B LEE
ATTN: D SIMONS
ATTN: LIBRARY

LOGICON R & D ASSOCIATES
ATTN: D CARLSON

LOGICON R & D ASSOCIATES
ATTN: B KILLIAN
ATTN: G GANONG
ATTN: J WALTON

MAXWELL LABORATORIES INC
ATTN: C PETERSEN
ATTN: K D PYATT JR
ATTN: P COLEMAN
ATTN: S PEYTON

MAXWELL LABS, INC
ATTN: J SEVIGNY

MISSION RESEARCH CORP
ATTN: B GOPLEN

NEW MEXICO ENGINEERING RESEARCH INSTITUTE
ATTN: J JARPE
ATTN: KENNETH BELL
ATTN: LIBRARY
ATTN: T MCCARSON

PHYSICS INTERNATIONAL CO
ATTN: C STALLINGS
ATTN: P SINCERNY

PULSE SCIENCES, INC
ATTN: P W SPENCE

S-CUBED
ATTN: C NEEDHAM

SCIENCE APPLICATIONS INTL CORP
ATTN: C HSIAO
ATTN: G EGGUM
ATTN: H WILSON
ATTN: R ALLEN
ATTN: TECHNICAL REPORT SYSTEM

SCIENCE APPLICATIONS INTL CORP
ATTN: W LAYSON

SCIENCE APPLICATIONS INTL CORP
ATTN: K SITES

SCIENCE APPLICATIONS INTL CORP
ATTN: G BINNINGER

SCIENCE RESEARCH LAB
2 CY ATTN: S FLUGHUM

SRI INTERNATIONAL
ATTN: A FLORENCE
ATTN: D KEOUGH
ATTN: J GIOVANOLA
ATTN: J SIMONS
ATTN: M SANAI
ATTN: P DE CARLI

TETRA CORP
ATTN: W MOENY

TEXAS TECH UNIVERSITY
ATTN: DR M KRISTIANSEN

TITAN CORPORATION (THE)
ATTN: R ENGLAND

TITAN RESEARCH & TECHNOLOGY DIVISION
ATTN: J THOMSEN

TRW INC
ATTN: TIC

TRW SPACE & DEFENSE SECTOR
ATTN: W WAMPLER

W J SCHAFER ASSOCIATES, INC
ATTN: E ALCARAZ

WASHINGTON STATE UNIVERSITY
2 CY ATTN: PROF Y GUPTA

WESTINGHOUSE ELECTRIC CORP
ATTN: J S FLETCHER

WESTINGHOUSE STC
ATTN: DR A H COOKSON

DIRECTORY OF OTHER

AUBURN UNIVERSITY
ATTN: M ROSE

UNIVERSITY OF NEW YORK-BUFFALO
ATTN: R DOLLINGER

UNIVERSITY OF CALIFORNIA-DAVIS
ATTN: J S DEGROOT